IMA Journal of Applied Mathematics (2021) **86**, 944–983
https://doi.org/10.1093/imamat/hxab035
Advance Access publication on 3 August 2021

Localized patterns in a generalized Swift–Hohenberg equation with a quartic marginal stability curve†

David C. Bentley and Alastair M. Rucklidge*
School of Mathematics, University of Leeds, Leeds LS2 9JT, UK
*Corresponding author: A.M.Rucklidge@leeds.ac.uk
†This paper is dedicated to the memory of Thomas Wagenknecht (1974–2012).

[Received on 2 November 2020; revised on 14 June 2021; accepted on 22 June 2021]

In some pattern-forming systems, for some parameter values, patterns form with two wavelengths, while for other parameter values, there is only one wavelength. The transition between these can be organized by a codimension-three point at which the marginal stability curve has a quartic minimum. We develop a model equation to explore this situation, based on the Swift–Hohenberg equation; the model contains, amongst other things, snaking branches of patterns of one wavelength localized in a background of patterns of another wavelength. In the small-amplitude limit, the amplitude equation for the model is a generalized Ginzburg–Landau equation with fourth-order spatial derivatives, which can take the form of a complex Swift–Hohenberg equation with real coefficients. Localized solutions in this amplitude equation help interpret the localized patterns in the model. This work extends recent efforts to investigate snaking behaviour in pattern-forming systems where two different stable non-trivial patterns exist at the same parameter values.

Keywords: pattern formation; quartic minimum; two wavelengths; localized patterns.

2020 Math Subject Classification: 35B36; 35B32; 37G05; 37L10.

1. Introduction

Pattern formation most commonly occurs with a single wavelength, as in for example zebra stripes, Rayleigh–Bénard convection and the Taylor–Couette flow (Hoyle, 2006). In these examples, there is a featureless basic state that loses stability to waves with a non-zero wavelength as a control parameter is increased. Typically the marginal stability curve, which separates stable from unstable waves depending on their wavelength and the control parameter, has a quadratic minimum.

In recent years, it has been recognized that pattern formation with two length scales can lead to a wide variety of complex and interesting patterns, such as superlattice patterns, quasipatterns and spatio-temporal chaos (see for example Castelino *et al.*, 2020, and references therein). Having two length scales can arise in different ways: in the Faraday wave problem with multi-frequency forcing, for example, patterns with the two length scales arise in response to different components of the forcing (Edwards & Fauve, 1994; Rucklidge & Silber, 2009; Skeldon & Rucklidge, 2015; Topaz & Silber, 2002). Another possibility is that the quadratic minimum in the marginal stability curve can change to a quadratic maximum with two nearby quadratic minima at the two length scales. This transition can occur via a quartic minimum, and is found in the magnetized Taylor–Couette experiement (Mamatsashvili *et al.*, 2019; Stefani *et al.*, 2009), Lapwood–Prats convection (Rees & Mojtabi, 2013), binary phase field

crystals (Holl *et al.*, 2021), surface waves in ferrofluids (Raitt & Riecke, 1997) and nonlinear optics (Kozyreff *et al.*, 2009). This paper is concerned first with developing and analyzing a model that contains this transition in as simple a form as possible, and second with investigating localized patterns in the model.

Problems with a single length scale where the pattern-forming bifurcation is subcritical can have parameter intervals where both the featureless and the patterned solutions are stable. In this case, it is possible to find localized solutions consisting of a region of a spatially periodic pattern embedded in a spatially homogeneous background (see Dawes, 2010; Knobloch, 2015, for reviews). With two length scales, there is a wider variety of possibilities, including having patterns with one wavelength embedded in a pattern with a different wavelength. This phenomenon has been observed in Rayleigh–Bénard convection in a long, thin channel or slot (Hegseth *et al.*, 1992), in large-aspect-ratio thermosolutal convection (Spina *et al.*, 1998), and has been explored in the context of generalized Ginzburg–Landau models (Bortolozzo *et al.*, 2006; Kozyreff *et al.*, 2009; Raitt & Riecke, 1995, 1997; Riecke, 1990).

A useful mathematical tool for studying pattern formation is the construction of model equations that display qualitatively similar behaviour as the physical system under consideration, but whose analysis is more tractable. Perhaps the most ubiquitous of such model equations is the Swift–Hohenberg (SH) equation (Swift & Hohenberg, 1977), originally introduced as a model of thermal fluctuations near the onset of Rayleigh–Bénard convection. It has been used extensively in the study of localized patterns, starting with the work of Hilali *et al.* (1995), Crawford & Riecke (1999) and Woods & Champneys (1999). The equation (in one dimension) is

$$\frac{\partial u}{\partial t} = \mu u - \left(1 + \frac{\partial^2}{\partial x^2}\right)^2 u + n_2 u^2 + n_3 u^3, \tag{1.1}$$

where $u(x,t) \in \mathbb{R}$ is an order parameter that represents the pattern, μ is the driving parameter and n_2 and n_3 are parameters controlling the nonlinear terms (typically $n_3 = -1$). We consider equation (1.1) subject to periodic boundary conditions on a domain $x \in [0, L]$.

The featureless (or trivial) solution $u = 0$ is stable for $\mu < 0$. Small amplitude perturbations of the form $e^{\sigma t + ikx}$ grow as $\sigma = \mu - \left(1 - k^2\right)^2$, so for $\mu > 0$ the maximum growth rate is at critical wavenumber $k = 1$ (independent of μ), and if $\mu > 0$, a range of wavenumbers will grow exponentially until nonlinear effects become important. The marginal stability curve is found by setting $\sigma = 0$, so

$$\mu = \left(1 - k^2\right)^2,$$

which has a quadratic minimum at $k = 1$. At $\mu = 0$ the trivial solution undergoes a pitchfork bifurcation, creating a branch of spatially periodic solutions, which is stable if it is supercritical, and unstable if not.

In large domains ($L \gg 1$), and with small amplitude solutions ($u = \mathcal{O}(\epsilon)$), standard weakly nonlinear theory can be applied. The pattern is written, with scaled space, time and parameter, as

$$u(x,t) = \epsilon A(X,T)e^{ix} + \text{c.c.} + \text{h.o.t.}, \quad X = \epsilon x, \quad T = \epsilon^2 t, \quad \mu = \epsilon^2 \mu_2, \tag{1.2}$$

where c.c. refers to the complex conjugate and h.o.t. refers to higher-order terms. In this limit, the solvability condition for A at third-order in ϵ results in the Ginzburg–Landau (GL) equation (Cross & Hohenberg, 1993):

$$A_T = \mu_2 A + 4A_{XX} + \left(3n_3 + \tfrac{38}{9}n_2^2\right)|A|^2 A, \tag{1.3}$$

where subscripts T and X refer to partial derivatives. This equation governs the long-wavelength slow evolution of the amplitude of solutions of (1.1). We define the coefficient of the nonlinear term

$$n_{SH} = 3n_3 + \tfrac{38}{9}n_2^2,$$

which determines the criticality of the bifurcation at $\mu = 0$: if $n_{SH} < 0$ the bifurcation is supercritical, and if $n_{SH} > 0$, the bifurcation is subcritical. In the supercritical case, the GL equation gives nonlinear stability of striped patterns to long-wavelength perturbations (the Eckhaus instability, see Eckhaus, 1965). In the subcritical case, the GL equation allows localized sech-profile solutions to equation (1.1) that can be continued in μ, leading to the well known homoclinic "snaking" structure of localized solutions of the Swift–Hohenberg and many other pattern-forming problems (Beck *et al.*, 2009; Burke & Knobloch, 2006, 2007b; Chapman & Kozyreff, 2009; Coullet *et al.*, 2000; Kozyreff & Chapman, 2006; Woods & Champneys, 1999).

The GL equation (1.3) is one standard tool useful in the analysis of the SH equation (1.1). There are three others that we mention briefly. First, the SH equation as written above is variational in time, and admits a Lyapunov functional:

$$\mathcal{F}[u] = \int_0^L \left(-\tfrac{1}{2}\mu u^2 + \tfrac{1}{2}\left(\left(1+\partial_x^2\right)u\right)^2 - \tfrac{1}{3}n_2 u^3 - \tfrac{1}{4}n_3 u^4\right) dx. \tag{1.4}$$

With $n_3 < 0$, it can easily be shown that $\mathcal{F}[u]$ is bounded below and that it is a decreasing function of time:

$$\frac{d\mathcal{F}}{dt} = -\int_0^L \left(\frac{\partial u}{\partial t}\right)^2 dx \leq 0.$$

Equilibrium states correspond to stationary points of $\mathcal{F}$, and those coinciding with local minima of $\mathcal{F}$ must necessarily be stable. A front connecting two patterns with different values of $\mathcal{F}$ will tend to move towards (and so eliminate) the pattern with the larger value. Localized solutions are found near the Maxwell point, where the pattern and the zero state have the same value of $\mathcal{F}$, and near this point the difference in $\mathcal{F}$ is small enough that the front becomes pinned (Pomeau, 1986) to the underlying pattern.

The second tool is the observation that the steady Swift–Hohenberg equation (1.1) admits a first integral in space. Multiplying the time-independent version of (1.1) through by $-u_x$, and integrating with respect to x, yields

$$\begin{aligned}\mathcal{H} &= -\int \left(\mu u - u - 2u_{xx} - u_{xxxx} + n_2 u^2 + n_3 u^3\right) u_x dx \\ &= -\tfrac{1}{2}(\mu - 1)u^2 + u_x^2 - \tfrac{1}{2}u_{xx}^2 + u_x u_{xxx} - \tfrac{1}{3}n_2 u^3 - \tfrac{1}{4}n_3 u^4,\end{aligned}$$

and so $\frac{d\mathcal{H}}{dx} = 0$. The quantity $\mathcal{H}$ is sometimes referred to as the Hamiltonian for the steady version of (1.1), since there is a change of coordinates under which the system has Hamiltonian structure. If there is a steady front connecting two patterns, the condition $\frac{d\mathcal{H}}{dx} = 0$ means that the two patterns must have the same value of $\mathcal{H}$.

The third useful tool is to note, again for the time-independent version of (1.1), that there is a Hamiltonian–Hopf bifurcation in space as μ crosses zero. At the bifurcation point, there is a pair of double spatial eigenvalues $\pm i$, and the normal form can be written as a pair of first-order ODEs in x for two complex variables. A bifurcation analysis performed by Iooss & Pérouème (1993) and Iooss & Adelmeyer (1998), and extended by Woods & Champneys (1999), provides a geometrical interpretation of the solutions of the normal form. In particular, there are parameter values where there are solutions of the SH equation that are homoclinic to the origin as $x \to \pm\infty$ (Burke & Knobloch, 2007a): these homoclinic orbits represent localized solutions.

The existence and bifurcation structure of localized solutions in the Swift–Hohenberg equation is now well understood: see Dawes (2010) and Knobloch (2015) for reviews. In this paper, we consider a generalized version of the Swift–Hohenberg equation that allows a quartic minimum of the marginal stability curve (§2). Unfolding this quartic minimum, and using tools such as generalized versions of the Ginzburg–Landau equation (§3), the Lyapunov function and the first integral introduced above (§4), allows us to identify parameter regimes where we can find patterns of one wavenumber localized in a background of patterns with a different wavenumber (§5). We compare our work to a derivation of the amplitude equation for a related problem, the Lugiato–Lefever equation, in §6. We discuss the significance of our results in §7. We include normal form calculations in Appendix A, but we have not found first integrals of the normal form, and so we have not been able to put it to immediate use.

2. The model equation

In this section, we build a model equation to explore the unfolding of the quartic minimum in the marginal stability curve. We start with the SH equation (1.1), modified to allow a marginal stability that can change from having one to having two minima, and then add a selection of nonlinear terms.

2.1 *Linear terms*

As a starting point, we consider a linear part of the PDE based on the polynomial

$$p_0(K) = (1 - K)^4,$$

where $K = k^2$. This is the simplest polynomial that has quartic minima at $k = \pm 1$. In the model equation, $1 - K$ will become $1 + \partial_{xx}$. The quartic minimum at $K = 1$ can be unfolded by adding two small terms to the equation, yielding

$$p(K) = p_0(K) + f_1 K + f_2 K^2, \tag{2.1}$$

with $f_1 = f_2 = 0$ at the quartic minimum. In principle, small terms $f_0, f_3 K^3$ and $f_4 K^4$ could be added as well, but f_0 can be absorbed into the bifurcation parameter μ, f_3 can be eliminated by making a small shift in K by $-\frac{1}{4} f_3$, and f_4 can be absorbed by an overall scaling.

Before writing down the PDE model, we consider the transition from having one minimum to two. The condition that $p(K)$ has two minima with a maximum in between is the same as the condition that

the derivative $p'(K)$ has three distinct real roots. Now

$$p'(K) = 4K^3 - 12K^2 + (2f_2 + 12)K + f_1 - 4,$$

and the condition that a cubic polynomial has three distinct real roots is that its discriminant should be positive. The boundary, where the discriminant is zero, occurs where

$$f_1^2 + 4f_1f_2 + 4f_2^2 + \tfrac{8}{27}f_2^3 = 0, \quad \text{or} \quad f_1 = -2f_2 \pm \left(-\tfrac{2}{3}f_2\right)^{\frac{3}{2}}.$$

In addition, when the discriminant is positive, $p(K)$ has two minima at K_1 and K_3 with a maximum at K_2 in between, with $K_1 < K_2 < K_3$, $K_1 + K_2 + K_3 = 3$ and $K_1K_2K_3 = 1 - \frac{1}{4}f_1$ (found from the relationship between the roots and coefficients of the cubic $p'(K) = 0$). Manipulating the conditions $p'(K_1) = 0$, $p'(K_3) = 0$ and $p(K_1) = p(K_3)$ leads to the conclusion that the two minima are equal when

$$K_1 + K_3 = 2, \quad K_2 = 1, \quad \text{and} \quad f_1 + 2f_2 = 0,$$

that is, the intermediate maximum is at $K = 1$ and the two minima are equally spaced on each side.

The next step is to convert the polynomial to the linear operator of the model equation:

$$\frac{\partial u}{\partial t} = \mu u - \left(1 + \frac{\partial^2}{\partial x^2}\right)^4 u + f_1\frac{\partial^2 u}{\partial x^2} - f_2\frac{\partial^4 u}{\partial x^4}.$$

A mode $u = e^{\sigma t + ikx}$ has growth rate $\sigma = \mu - (1 - k^2)^4 - f_1k^2 - f_2k^4 = \mu - p(k^2)$, connecting the dispersion relation to the polynomial $p(K)$ discussed above. Marginal stability, when $\sigma = 0$, occurs when $\mu = p(k^2)$, and Figure 1 shows examples of the marginal stability curves in the $(f_1 + 2f_2, f_2)$ parameter plane. The discriminant is positive, and there is a double minimum, within the cusp-shaped region below the solid curves, and the two minima are equal on the dashed line. The cusp, the point at which there is a quartic minimum with $f_1 = f_2 = 0$, represents a codimension-three bifurcation as μ crosses zero.

However, a model based solely on this would have a wavenumber for maximum growth rate for solutions that did not depend on μ. Regions of secondary instability of patterns are organized around the curve of maximum growth rate, and it is important that this curve is modelled correctly. In pattern-forming problems with a quadratic minimum, the wavenumber for maximum growth rate typically depends only linearly on μ, so with $\mu \ll 1$, this lack of dependence on μ in the SH equation is reasonable. However, with a quartic minimum, Proctor (1991) argues that additional terms should be included in the unfolding of a quartic minimum in order to allow the wavenumber of maximum growth rate to depend on μ. For this reason, we propose the modified linear operator

$$\frac{\partial u}{\partial t} = \mu\left(1 + \mu_p\left(1 + \frac{\partial^2}{\partial x^2}\right)\right)u - \left(1 + \frac{\partial^2}{\partial x^2}\right)^4 u + f_1\frac{\partial^2 u}{\partial x^2} - f_2\frac{\partial^4 u}{\partial x^4}, \tag{2.2}$$

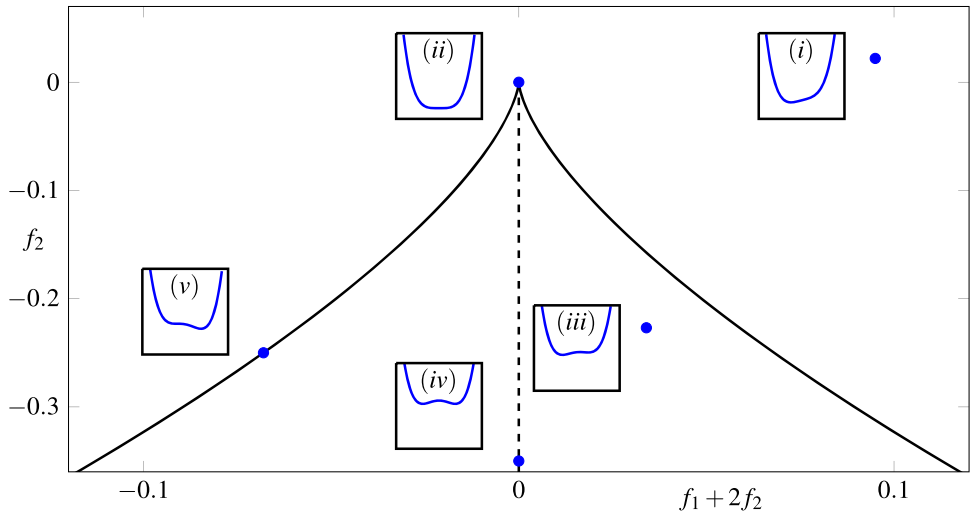

FIG. 1. Five examples of the marginal stability curves $\mu = p(K)$ in different regions of the $(f_1 + 2f_2, f_2)$ parameter space. The curves (blue in black boxes) shown are: (*i*) single minimum, (*ii*) quartic minimum, (*iii*) double minima, with the left minimum being the lower, (*iv*) double minima, with both minima at the same height, and (*v*) a single minimum and an inflexion point. The specific parameters for each example are shown as blue dots. The solid lines indicate where the discriminant is zero (the derivative has a double zero), and the dashed line ($f_1 + 2f_2 = 0, f_2 < 0$) indicates where the two minima exist and have the same height.

where we will call the extra term, proportional to μ_p, the Proctor term, although the form of this extra term differs from that proposed by Proctor (1991). The dispersion relation is now

$$\sigma = \mu\left(1 + \mu_p\left(1 - k^2\right)\right) - \left(1 - k^2\right)^4 - f_1 k^2 - f_2 k^4,$$

and so

$$\frac{d\sigma}{dk^2} = -\mu\mu_p + 4\left(1 - k^2\right)^3 - f_1 - 2f_2 k^2.$$

The curve of maximum (or minimum) growth rate is then defined by $\frac{d\sigma}{dk^2} = 0$, i.e.,

$$\mu = \frac{1}{\mu_p}\left(4\left(1 - k^2\right)^3 - f_1 - 2f_2 k^2\right).$$

For $\mu_p \neq 0$ and $f_1 = f_2 = 0$ (Figure 2*a*), this curve of maximum growth rate is a cubic and so is tangent to the neutral stability curve, while for non-zero f_1 and f_2 (Figure 2*b*), the curves of maximum growth rate intersect the two minima in the marginal stability curve transversally.

Including the Proctor term influences the shape of the marginal stability curve. Throughout most of this paper we will assume that μ_p is small enough not to influence the behaviour of solutions, apart from the asymptotic analysis in §3.3 (where the Proctor term necessarily appears as a higher order term), and a numerical consideration in §5.2.

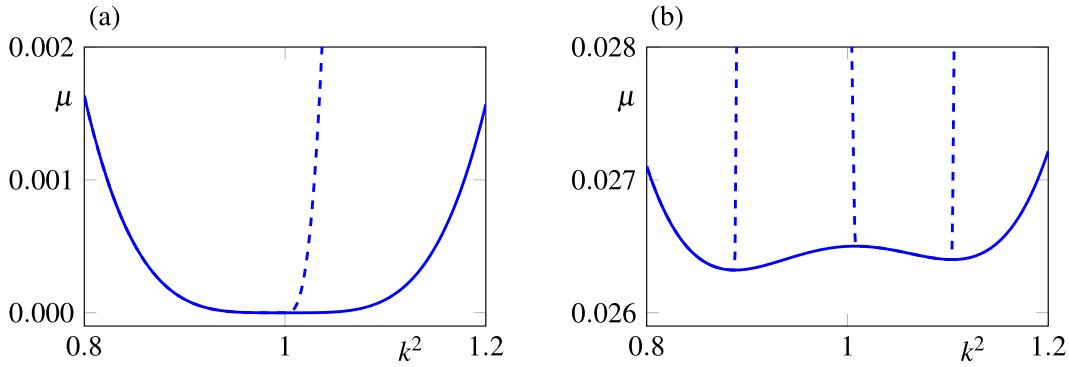

FIG. 2. Marginal stability curve (solid) and curve of maximum (or minimum) growth (dashed) for (2.2), for (a) $f_1 = f_2 = 0$, and (b) $f_1 = 0.05$ and $f_2 = -0.0235$. The coefficient $\mu_p = -0.1$ in both cases. Two of the three dashed lines in (b) join together above the top of the frame.

The linear part of the model derived so far is symmetric under spatial reversals, i.e., x and $-x$ are equivalent. Some systems break reflection symmetry, for example, the Taylor–Couette system in the presence of an azimuthal and axial magnetic field (Mamatsashvili *et al.*, 2019; Stefani *et al.*, 2009); this can be modelled by including terms such as $\left(f_{d0} - f_{d1}\partial_{xx}\right) u_x$, leading to drifting solutions. However, the reflection symmetry is useful in the analysis of the model equation, so we do not include drift terms here.

2.2 *Nonlinear terms*

Nonlinear terms in the model will saturate exponentially growing solutions at finite amplitude, and should respect the symmetry (or lack thereof) of any underlying physical systems. The usual SH nonlinear term is $-u^3$, allowing $u \to -u$ symmetry, but here we break this symmetry and chose

$$n_2 u^2 + n_3 u^3.$$

as nonlinear terms for the model. There are many more possibilities for nonlinear terms, both with and without variational structure, that have been used by many authors (Burke & Dawes, 2012; Crawford & Riecke, 1999; Knobloch, 1990; Rucklidge *et al.*, 2012) for similar equations in different contexts. For the purposes of this paper, we consider only the nonlinear terms above, retaining the coefficients n_2 and n_3 as parameters. We focus on the case where the bifurcation is supercritical, which limits the range of values that n_2 and n_3 can take. In particular, we must have

$$n_A \equiv 3n_3 + \tfrac{326}{81} n_2^2 < 0, \tag{2.3}$$

derived in §3.1. For numerical examples, we will take $n_2 = 0.1$ and $n_3 = -1$ throughout.

We now have our complete model equation, written here with the Proctor term

$$\frac{\partial u}{\partial t} = \mu\left(1 + \mu_p\left(1 + \frac{\partial^2}{\partial x^2}\right)\right)u - \left(1 + \frac{\partial^2}{\partial x^2}\right)^4 u + f_1 \frac{\partial^2 u}{\partial x^2} - f_2 \frac{\partial^4 u}{\partial x^4}, + n_2 u^2 + n_3 u^3, \tag{2.4}$$

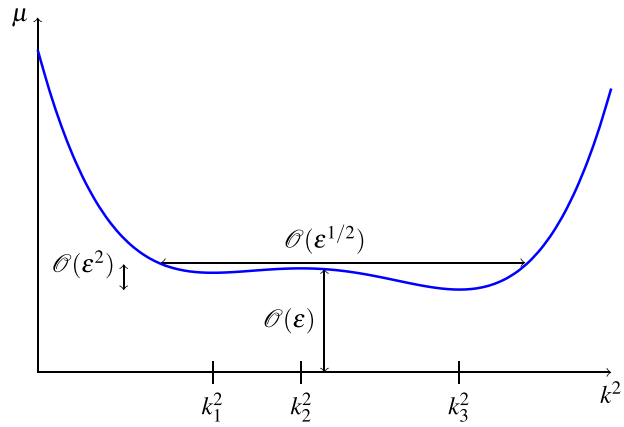

FIG. 3. Scalings used for the asymptotic analysis. The deviations from a quartic minimum are contained in a $\mathcal{O}(\epsilon^{1/2}) \times \mathcal{O}(\epsilon^2)$ box, and the whole curve is shifted by an $\mathcal{O}(\epsilon)$ amount.

and without

$$\frac{\partial u}{\partial t} = \mu u - \left(1 + \frac{\partial^2}{\partial x^2}\right)^4 u + f_1 \frac{\partial^2 u}{\partial x^2} - f_2 \frac{\partial^4 u}{\partial x^4} + n_2 u^2 + n_3 u^3. \tag{2.5}$$

For the remainder of this paper, we will concentrate mostly on the parameter values where the marginal stability curves have two minima and there is bistability between patterns of different wavelength, leading to the possibility of these patterns coexisting in separate parts of the domain. Although these equations are related to the two length scale models of Lifshitz & Petrich (1997) and Rucklidge *et al.* (2012), our model cannot be derived from these simply by setting the two length scales to be equal.

3. Weakly nonlinear analysis

In this section, we compute weakly nonlinear solutions for the model (2.5) by deriving a generalized version of the Ginzburg–Landau equation, and use it to establish where one-dimensional periodic patterns are stable to long-wave perturbations. For most of the calculations we set $\mu_p = 0$, but we do consider the effect of the Proctor term briefly in §3.3.

3.1 *Derivation of a generalized Ginzburg–Landau equation*

For the model PDE (2.5), we consider only situations where we have a small perturbation of the quartic marginal stability curve. We focus on the case where the perturbed marginal stability curve has two minima, below the cusp (solid lines) in Figure 1. At the quartic minimum, an appropriate scaling is that if the solution u is of $\mathcal{O}(\epsilon)$, then the slow time T and long length X should be $\mathcal{O}(\epsilon^2)$ and $\mathcal{O}(\epsilon^{1/2})$ respectively: the long length X is even longer than the $\mathcal{O}(\epsilon)$ scaling in the case of a quadratic minimum in (1.2). We therefore restrict f_1 and f_2 such that the two minima in the marginal stability curve lie in an $\mathcal{O}(\epsilon^{1/2}) \times \mathcal{O}(\epsilon^2)$ box, as illustrated in Figure 3. Other scalings are possible.

To simplify the form of the marginal stability curve, we take $\mu_p = 0$ and consider the two minima and intermediate maximum of the function $\mu = p(k^2)$ in (2.1). The condition for an extremum is

$p'(K) = 0$, with $K = k^2$: writing $\frac{1}{4}p'(K)$ as $(k^2 - k_1^2)(k^2 - k_2^2)(k^2 - k_3^2)$, with $k_1 < k_2 < k_3$, leads to the conclusion that

$$k_1^2 + k_2^2 + k_3^2 = 3, \qquad k_1^2k_2^2 + k_1^2k_3^2 + k_2^2k_3^2 = 3 + \tfrac{1}{2}f_2, \qquad k_1^2k_2^2k_3^2 = 1 - \tfrac{1}{4}f_1. \tag{3.1}$$

To satisfy these three equations, we introduce new parameters γ and δ, defined by

$$k_1^2 = 1 - \gamma - \tfrac{1}{2}\delta, \qquad k_2^2 = 1 + 2\gamma, \qquad k_3^2 = 1 - \gamma + \tfrac{1}{2}\delta, \tag{3.2}$$

such that the first equation in (3.1) is satisfied. Requiring $k_1 < k_2 < k_3$ implies $\delta > 6|\gamma| \geq 0$. Substituting (3.2) into the second and third equations in (3.1) yields

$$k_1^2k_2^2 + k_1^2k_3^2 + k_2^2k_3^2 = 3 - 3\gamma^2 - \tfrac{1}{4}\delta^2 = 3 + \tfrac{1}{2}f_2,$$
$$k_1^2k_2^2k_3^2 = 1 - 3\gamma^2 - \tfrac{1}{4}\delta^2 - \tfrac{1}{2}\gamma\delta^2 + 2\gamma^3 = 1 - \tfrac{1}{4}f_1.$$

These are rearranged to result in expressions for f_1, f_2 and $f_1 + 2f_2$ in terms of γ and δ:

$$f_1 = 12\gamma^2 + \delta^2 + 2\gamma\delta^2 - 8\gamma^3, \qquad f_2 = -6\gamma^2 - \tfrac{1}{2}\delta^2, \qquad f_1 + 2f_2 = 2\gamma\left(\delta^2 - 4\gamma^2\right).$$

The restriction $\delta > 6|\gamma|$ means that $\delta^2 - 4\gamma^2 > 0$, and so $f_1 + 2f_2 = 0$ implies $\gamma = 0$ and $k_2 = 1$.

Now, if the minima and maxima of the marginal stability curve are to satisfy the scalings in Figure 3, we need $\delta = \mathcal{O}(\epsilon^{1/2})$ and γ no larger than this. We also need $p(k_2^2) - p(k_1^2)$ and $p(k_2^2) - p(k_3^2)$ to be $\mathcal{O}(\epsilon^2)$:

$$p(k_2^2) - p(k_1^2) = \tfrac{1}{16}(\delta - 2\gamma)(\delta + 6\gamma)^3, \qquad p(k_2^2) - p(k_3^2) = \tfrac{1}{16}(\delta + 2\gamma)(\delta - 6\gamma)^3,$$

so with $\delta = \mathcal{O}(\epsilon^{1/2})$ and γ no larger, these differences fit within $\mathcal{O}(\epsilon^2)$. The overall marginal stability curve is shifted up by an amount $p(1) \approx \frac{1}{2}\left(12\gamma^2 + \delta^2\right) = \mathcal{O}(\epsilon)$, again within the scalings indicated in Figure 3. The scaling of γ and δ imply f_1 and f_2 are both $\mathcal{O}(\epsilon)$, but that $f_1 + 2f_2 = \mathcal{O}(\epsilon^{3/2})$.

We are now in a position to perform the multiple scales analysis. The full set of scalings used are

$$\begin{aligned} u &= \sum_{n=2}^{6} \epsilon^{n/2} u_{n/2}, & \mu &= \epsilon\mu_1 + \epsilon^2\mu_2, \\ \partial_t &= \epsilon^2\partial_T, & f_1 &= \epsilon f_1, \\ \partial_x &= \partial_x + \epsilon^{1/2}\partial_X, & f_2 &= \epsilon f_2, \qquad \text{with } f_1 + 2f_2 = \mathcal{O}(\epsilon^{3/2}), \end{aligned} \tag{3.3}$$

where $\epsilon\mu_1$ is the amount by which the marginal stability curve is shifted. We also define a singular linear operator $\mathcal{L}$ to be $(1 + \partial_x^2)^4$, with $\mathcal{L}e^{\pm ix} = 0$.

Inserting these scalings into (2.5), we obtain at leading order $\mathcal{O}(\epsilon)$:

$$0 = -\mathcal{L}u_1,$$

which is satisfied by taking

$$u_1 = A(X,T)e^{ix} + \text{c.c.}, \tag{3.4}$$

where c.c. represents the complex conjugate. It is useful to observe that $\partial_x^2 u_1 = -u_1$.

Proceeding to $\mathcal{O}(\epsilon^{3/2})$, we have

$$0 = -\mathcal{L}u_{3/2} - 8\partial_{xX}\underbrace{(1+\partial_x^2)^3 u_1}_{=0}.$$

The most convenient way to solve this is to set $u_{3/2} = 0$.

At $\mathcal{O}(\epsilon^2)$, we have

$$0 = \mu_1 u_1 - \mathcal{L}u_2 - 4\partial_X^2\underbrace{\left(1+9\partial_x^2+15\partial_x^4+7\partial_x^6\right)u_1}_{=0} + f_1\partial_x^2 u_1 - f_2\partial_x^4 u_1 + n_2 u_1^2.$$

The terms proportional to e^{ix} have a prefactor of $\mu_1 - (f_1+f_2)$ We need to eliminate these terms in order to solve for u_2, which we do by setting $\mu_1 = f_1+f_2$. With this, the remaining terms are $0 = -\mathcal{L}u_2 + n_2 u_1^2$, which can be solved to give

$$u_2 = n_2\left(\tfrac{1}{81}A^2 e^{2ix} + \tfrac{1}{81}\bar{A}^2 e^{-2ix} + 2|A|^2\right).$$

The factors $\frac{1}{81}$ come from $\mathcal{L}e^{2ix} = 81e^{2ix}$ when $\mathcal{L}$ is inverted.

At $\mathcal{O}(\epsilon^{5/2})$ we have

$$0 = -\mathcal{L}u_{5/2} - 8\partial_{xX}(1+\partial_x^2)^3 u_2 - 8\partial_x^3\partial_X\underbrace{(3+10\partial_x^2+7\partial_x^4)u_1}_{=0} + \underbrace{2f_1\partial_x\partial_X u_1 - 4f_2\partial_x^3\partial_X u_1}_{=2(f_1+2f_2)\partial_{xX}u_1}.$$

The only terms involving $e^{\pm ix}$ on the RHS are the two on the end that combine to have a prefactor of $f_1 + 2f_2$. As discussed above, this combination is a factor of $\epsilon^{1/2}$ smaller than f_1 and f_2 separately, so this term can be pushed to $\mathcal{O}(\epsilon^3)$ and dropped from this equation. With this, the two remaining terms in the equation can be solved for $u_{5/2}$:

$$u_{5/2} = \frac{32}{243}n_2\left(iAA_X e^{2ix} - i\bar{A}\bar{A}_X e^{-2ix}\right).$$

There is no constant term in $u_{5/2}$.

Finally, continuing to $\mathcal{O}(\epsilon^3)$, and including the term pushed from $\mathcal{O}(\epsilon^{5/2})$, we have

$$\begin{aligned}\partial_T u_1 = {} & \mu_1 u_2 + \mu_2 u_1 - \mathcal{L}u_3 - 8\partial_{xX}\left(1+\partial_x^2\right)^3 u_{5/2} \\ & - 4\partial_X^2\left(1+9\partial_x^2+15\partial_x^4+7\partial_x^6\right)u_2 - 2\partial_X^4\left(3+30\partial_x^2+35\partial_x^4\right)u_1 \\ & + f_1\partial_x^2 u_2 - f_2\partial_x^4 u_2 + f_1\partial_X^2 u_1 - 6f_2\partial_x^2\partial_X^2 u_1 + 2n_2 u_1 u_2 + n_3 u_1^3 \\ & + 2(f_1+2f_2)\partial_{xX}u_1.\end{aligned}$$

The solvability condition requires the elimination of all terms proportional to $e^{\pm ix}$. There are no contributions from $\mathcal{L}u_3$ and from the terms linear in u_2 and $u_{5/2}$. Recalling that $\partial_x^2 u_1 = -u_1$, the terms proportional to e^{ix} result in the solvability condition:

$$\frac{\partial A}{\partial T} = \mu_2 A + 2i\nu_1\frac{\partial A}{\partial X} + \nu_2\frac{\partial^2 A}{\partial X^2} - 16\frac{\partial^4 A}{\partial X^4} + \left(3n_3 + \tfrac{326}{81}n_2^2\right)|A|^2 A, \tag{3.5}$$

where $\nu_1 = f_1 + 2f_2$ and $\nu_2 = f_1 + 6f_2$. The nonlinear term is $n_A|A|^2A$, with n_A defined in (2.3). This is a generalization of the Ginzburg–Landau equation (1.3), and each term in the equation is, in terms of the original unscaled variables, of order $\mathcal{O}(\epsilon^3)$. The equation has the symmetry $(A, X) \to (\bar{A}, -X)$, which follows from the $x \to -x$ symmetry of the original problem and (3.4). Similar amplitude equations have been proposed before (Raitt & Riecke, 1995; Riecke, 1990; Riley & Davis, 1989), although not formally derived via an asymptotic expansion, to model other problems with very flat marginal stability curves. As we discuss in §6, setting $\nu_1 = 0$ and $\nu_2 < 0$ results in the complex Swift–Hohenberg equation with real coefficients (Gelens & Knobloch, 2010).

3.2 *Nonlinear stability of rolls*

We can find roll solutions to (3.5) easily, and use the equation to examine their stability to long wavelength Eckhaus instabilities. We restrict ourselves to the supercritical case, where the coefficient n_A of the nonlinear term is negative. We consider a roll solution at slightly off-critical wavenumber, i.e.,

$$A(X,T) = Re^{iqX}, \tag{3.6}$$

which corresponds to a solution $u = R\exp\left(i\left(1+\epsilon^{1/2}q\right)x\right)$ of (2.5) since $X = \epsilon^{1/2}x$, and $q = \mathcal{O}(1)$. These are also known as phase-winding solutions. Substituting (3.6) into (3.5), and rearranging, we obtain

$$R^2 = -\frac{1}{n_A}\left(\mu_2 - 2\nu_1 q - \nu_2 q^2 - 16q^4\right), \tag{3.7}$$

where $n_A < 0$ for a supercritical bifurcation. The existence boundary of rolls, which is also the marginal stability curve, is where $R^2 = 0$, or equivalently

$$\mu_2 = 2\nu_1 q + \nu_2 q^2 + 16q^4, \tag{3.8}$$

with ν_1 and ν_2 here playing the roles of unfolding parameters for the quartic minimum of the marginal stability curve.

To determine the stability of these roll solutions, we perturb (3.6), writing

$$A(X,T) = R\,(1 + r(X,T))\,e^{i(qX+\phi(X,T))},$$

where $|r|,|\phi| \ll 1$, following Hoyle (2006). We substitute this expressions into (3.5), linearize and separate the real and imaginary parts to obtain two linear constant coefficient PDEs for r and ϕ. To solve these, we seek solutions of the form $e^{\sigma T+imX}$, with $m \ll q$ and derive a quadratic equation for the growth rate σ. One root of this is always negative for a supercritical solution, and the other root is

$$\sigma = -m^2\left(\nu_2 + 96q^2 + \frac{2}{n_A R^2}\left(\nu_1 + \nu_2 q + 32q^3\right)^2\right) + \mathcal{O}(m^3).$$

See Bentley (2012) for details.

For the rolls to be unstable, we require $\sigma > 0$ for some m, giving a stability boundary defined by

$$R^2 = -2\frac{\left(\nu_1 + \nu_2 q + 32q^3\right)^2}{n_A\left(\nu_2 + 96q^2\right)},$$

and, recalling (3.7), we find the Eckhaus stability boundary

$$\mu_2 = 2\nu_1 q + \nu_2 q^2 + 16q^4 + \frac{2}{\nu_2 + 96q^2}\left(\nu_1 + \nu_2 q + 32q^3\right)^2. \tag{3.9}$$

Figure 4 shows an example of the marginal (3.8) and Eckhaus (3.9) curves. Inside the Eckhaus (dashed) curve, patterns are stable to long wavelength disturbances. Note that $\nu_2 < 0$ when there are two distinct minima, so (3.9) has two vertical asymptotes at $q = \pm\sqrt{-\nu_2/96}$. Between these asymptotes, μ_2 is below the marginal stability curve.

3.3 *The Proctor term*

The presence of these asymptotes means that the Eckhaus boundary does not close up in the middle, as might be expected. However, Proctor (1991) considered an amplitude equation similar to (3.5) but with the first term on the RHS replaced by $\mu_2(1 \pm i\partial_X)A$, and found that (depending on parameters) the inner edges of the left and right stability boundaries can meet, or the stability region can close with increasing μ with two separate stability regions, and the stability boundaries can be non-monotonic – see Proctor (1991) and Bentley (2012) for examples.

However, when we considered the model equation (2.4), with the Proctor term included, we encountered difficulties with the weakly nonlinear analysis. Writing $\mu = \epsilon\mu_1 + \epsilon^2\mu_2$, as in (3.3), turns out to be inadequate, so we modified the scaling to include an additional $\epsilon^{3/2}\mu_{3/2}\left(1 + \partial_x^2\right)$ term, aiming to relate $\mu_{3/2}$ to μ_p. It turns out that this does not work either, and possibly further (potentially higher order) terms would need to be considered for a consistent scaling (Bentley, 2012).

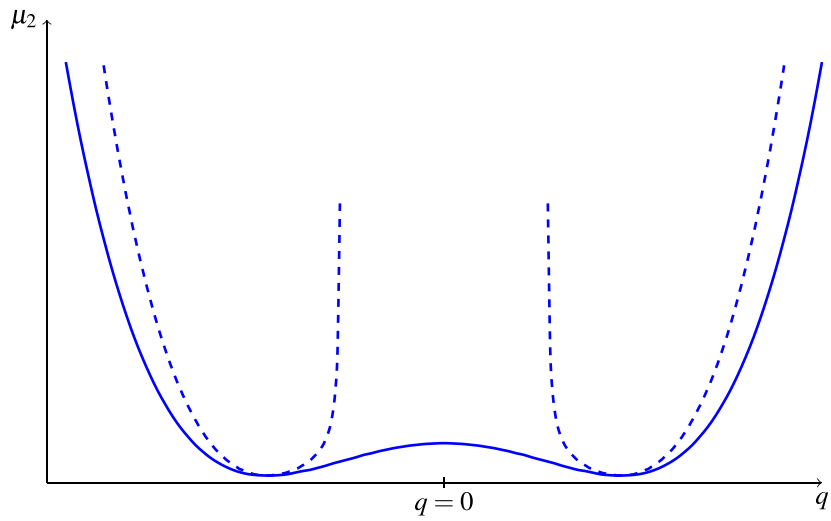

FIG. 4. Marginal stability curve (solid) and Eckhaus curves (dashed) for $\nu_1 = 0$ and $\nu_2 = -0.28$. The regions above the dashed curves are Eckhaus stable.

4. Lyapunov functional and the first integral

In the Swift–Hohenberg equation, the Lyapunov functional and first integral are useful for finding localized solutions: if two solutions are to be connected by a stationary front, they should have the same values of the first integral and similar values of the Lyapunov functional. In this section, we generalize the SH results to the model equation (2.5).

Multiplying the steady version of (2.5) by u_x and integrating by parts gives us a first integral:

$$\mathcal{H} = -\tfrac{1}{2}(\mu-1)u^2 - \tfrac{1}{3}n_2u^3 - \tfrac{1}{4}n_3u^4 + \tfrac{1}{2}(4-f_1)u_x^2 - \tfrac{1}{2}(6+f_2)\left(u_{xx}^2 - 2u_xu_{xxx}\right) + 2u_{xxx}^2 - 4u_{xx}u_{xxxx} + 4u_xu_{xxxxx} - \tfrac{1}{2}u_{xxxx}^2 + u_{xxx}u_{xxxxx} - u_{xx}u_{xxxxxx} + u_xu_{xxxxxxx}.$$

Any steady solution of (2.5) must have $\frac{d\mathcal{H}}{dx} = 0$. It is a straight-forward modification to include the Proctor term from (2.4).

Using the Lyapunov functional for the Swift–Hohenberg equation (1.4) as a starting point, we define a similar functional for (2.5), namely

$$\mathcal{F}[u] = \int_0^L \left(-\tfrac{1}{2}\mu u^2 + \tfrac{1}{2}\left(\left(1+\partial_x^2\right)^2 u\right)^2 + \tfrac{1}{2}f_1\left(\partial_x u\right)^2 + \tfrac{1}{2}f_2\left(\partial_x^2 u\right)^2 - \tfrac{1}{3}n_2u^3 - \tfrac{1}{4}n_3u^4\right)dx.$$

One can readily show that

$$\frac{\partial u}{\partial t} = -\frac{\delta\mathcal{F}}{\delta u} \qquad \text{and} \qquad \frac{d\mathcal{F}}{dt} = -\int_0^L \left(\frac{\partial u}{\partial t}\right)^2 dx \le 0.$$

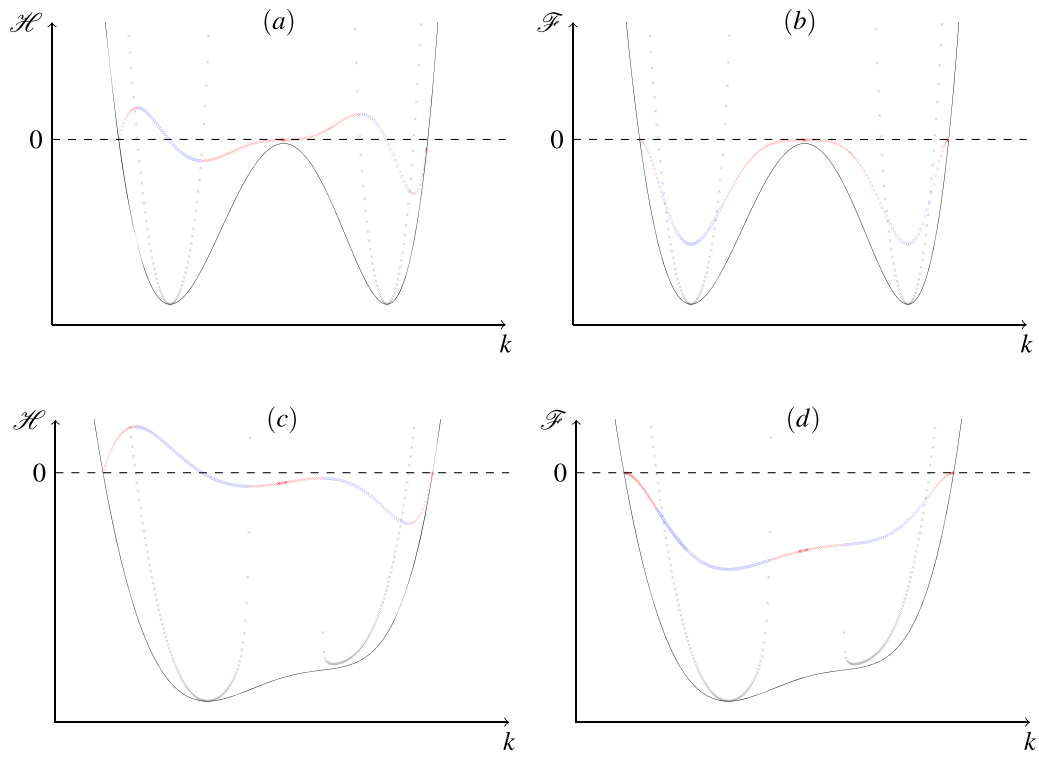

FIG. 5. Plot of $(a)30\mathcal{H}$ and $(b)3\times10^3\mathcal{F}$, against k, for $f_1 = 0.14, f_2 = -0.07$ and $\mu = 0.07$, computed using AUTO. (c,d): $15\mathcal{H}$ and $0.5\times10^3\mathcal{F}$, for $f_1 = 0.0488, f_2 = -0.0227$ and $\mu = 0.0306$. The red crosses correspond to Eckhaus unstable wavenumbers, and the blue circles to Eckhaus stable wavenumbers. The marginal stability curve (solid black) and Eckhaus curves (black crosses) are also shown – the change from red crosses to blue circles does not exactly match the Eckhaus boundary owing to the scaling of $\mathcal{H}$ and $\mathcal{F}$. Note that in (c,d) there is only one minimum in the marginal stability curve, but there is a region of Eckhaus-stable patterns above the almost-minimum.

It is possible to show that $\mathcal{F}[u]$ is bounded below provided $f_2 > -4$ and $n_3 < 0$ (Bentley, 2012), and so, as in the SH equation, that stable solutions are local minima of $\mathcal{F}[u]$. Similarly, it is a straight-forward modification to include the Proctor term from (2.4).

Small-amplitude solutions of (2.5) can be found using the generalized GL equation (3.5), and these can be used to find weakly nonlinear estimates of $\mathcal{H}$ and $\mathcal{F}$. Alternatively, fully nonlinear solutions of (2.5) can be found numerically, for example by using AUTO (Doedel, 2007). Examples of $\mathcal{H}$ and $\mathcal{F}$ computed numerically in this way are shown in Figure 5, in the cases where the minima in the marginal stability curve are at the same height, and where there is a single minimum with an almost-minimum just outside the cusp. These were computed using an initial solution on a domain of size $L = 2\pi$, which was then continued in L, increasing and decreasing to cover the range of wavenumbers for which a pattern solution exists. We note that $\mathcal{H}$ and $\mathcal{F}$ are both zero at the extremities of the existence region, and that the extrema of $\mathcal{H}$ correspond to the Eckhaus stability boundaries.

The third tool, mentioned in §1, is the normal form of this variant of the Hamiltonian–Hopf bifurcation with four-fold degenerate eigenvalues $\pm i$. We derive the normal form for this bifurcation

in Appendix A (see equations (A.9) and (A.10)), but as we have not found any first integrals of the normal form, we do not see a way to use it at this point.

5. Localized solutions

The first integral $\mathcal{H}$ and the Lyapunov functional $\mathcal{F}$ are two imporant tools for identifying where a pattern of one type can be localized within a background of a pattern of another type: the values of the first integral for the two patterns must be the same (since $\frac{d\mathcal{H}}{dx} = 0$ on any steady solution) and the Lyapunov functional for the two patterns should be approximately the same.

We see from the example in Figure 5(a,b) that there is a range of possible wavenumbers that satisfy the requisite criteria for patterns with two different wavenumbers coexisting, namely there are wavenumbers that have the same value of $\mathcal{H}$, and there are (different) wavenumbers with the same value of $\mathcal{F}$. To narrow down the allowable wavenumbers, we look for wavenumber pairs $(k_- < 1, k_+ > 1)$ such that $\mathcal{H}(k_-) = \mathcal{H}(k_+)$ and $\mathcal{F}(k_-) = \mathcal{F}(k_+)$. We do this by looking for intersections of contour lines plotted in the (k_+, k_-) plane. For the parameter values in Figure 5(a,b), a pair of wavenumbers that satisfy this condition are $(k_+, k_-) = (1.0778, 0.8839)$. We view such a point as an extension of the Maxwell point for the Swift–Hohenberg equation, though it plays a different role: in the Swift–Hohenberg the localized solutions are organized about the Maxwell point, whereas we use the extension merely as a starting point to look for localized solutions.

On a periodic domain of length L, wavenumbers are restricted to integer multiples of $k = 2\pi/L$. We therefore construct an initial condition consisting of a region of pattern with wavenumber close to 1.0778 embedded in a background of pattern with wavenumber close to 0.8839. Fixing a domain size $L = 64 \times 2\pi$, we choose $k_- = 58/64$ and $k_+ = 70/64$, and solve (2.5) using a second-order numerical scheme based on Exponential Time Differencing (Cox & Matthews, 2002). One example solution after transients can be seen in Figure 6, which demonstrates that localized solutions to (2.5) exist and are stable. This solution is made up of a high-wavenumber patch ($k \approx 1.0895$) in the centre of the domain, surrounded by low-wavenumber regions ($k \approx 0.9015$). The approximation to the local wavenumber in Figure 6(b) is found via

$$\text{local wavenumber} = \sqrt{\frac{-u_{xx}}{u}}, \tag{5.1}$$

and matches (at least approximately) the expected values. The oscillations seen in the amplitude and in the local wavenumber represent a beating between the two constituent wavenumbers k_- and k_+ as the pattern adjusts from one wavenumber to the other.

We can continue this and other solutions we have found in AUTO, continuing in μ to obtain the bifurcation diagram shown in Figure 7. Localized solutions lie on distinct branches that do not join up, created in saddle-node bifurcations. The solution branches corresponding to a pattern of single wavelength k_- or k_+ are included for reference. On localized solutions branches closer to the k_- branch, more of the domain is filled by the k_- pattern than the k_+ pattern, and *vice versa*. The localized solution branches extend to values of μ below the value at the local maximum of the marginal stability curve ($\mu(k_2) = 0.0699$).

We find similar disconnected branches of localized solutions even when the local minima in the marginal stability curve are not at the same height, and even just outside the cusp, where there is a single minimum and a second almost-minimum, as in Figure 5(c,d). Solutions in this region rely on

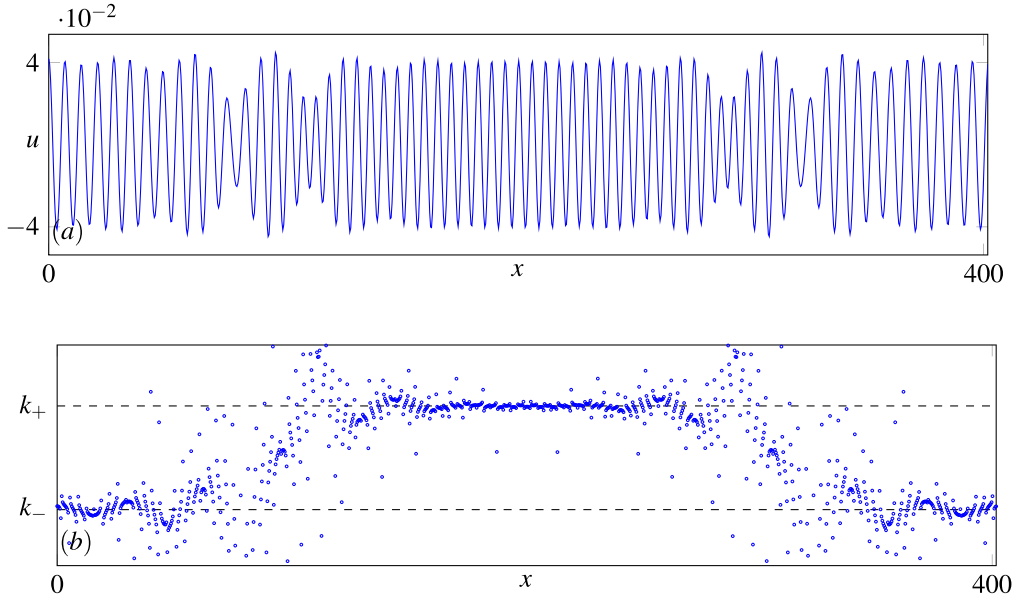

FIG. 6. Numerical simulation of mixed pattern initial condition with wavenumbers $k = 58/64 = 0.90625$ and $k = 70/64 = 1.09375$. The parameter values are: $f_1 = 0.14, f_2 = -0.07$ and $\mu = 0.07, n_2 = 0.1, n_3 = -1, L = 64 \times 2\pi$ and timestep 0.01. (a) final solution profile $u(x)$. (b) approximation to the local wavenumber, defined in (5.1). The values indicated are $k_- = 0.9015$ and $k_+ = 1.0895$.

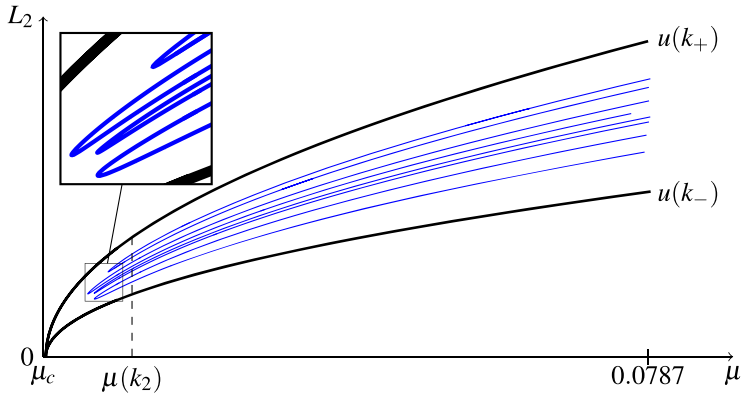

FIG. 7. Bifurcation diagram for parameter values $f_1 = 0.14, f_2 = -0.07$. The critical value of the bifurcation parameter μ is $\mu_c = 0.0687$, and the local maximum of the marginal stability curve occurs at $(k_2, \mu(k_2)) = (1, 0.0699)$. The thick black branches correspond to periodic patterns with wavenumbers k_-, k_+, and are given for reference. The blue branches correspond to localized solutions. Inset is a magnification of the saddle-nodes.

there being a region of Eckhaus-stable patterns still present above the almost-minimum, disconnected from the marginal stability curve.

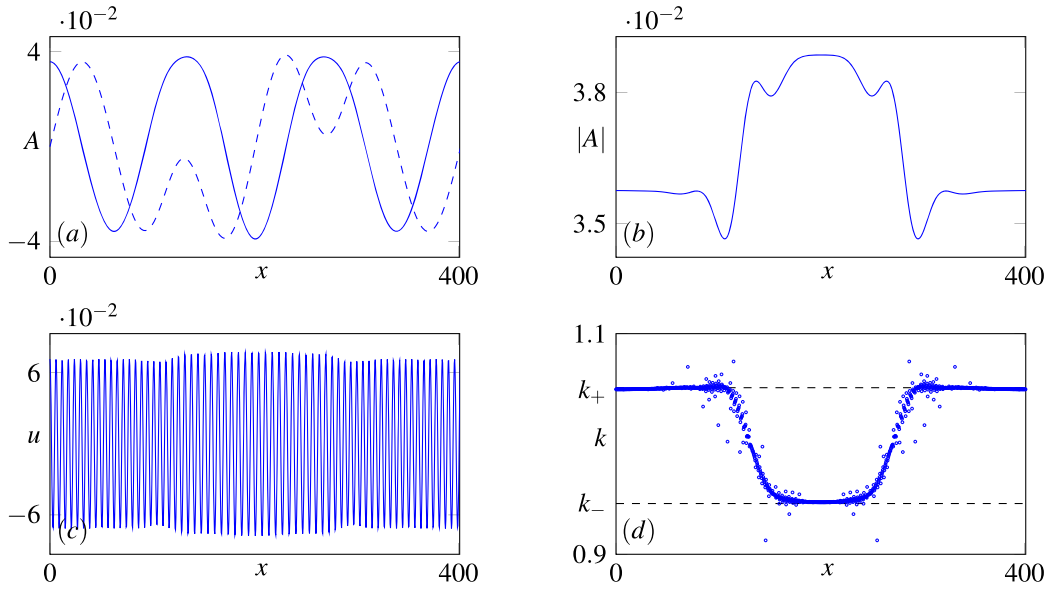

FIG. 8. Solution to (3.5), with $\nu_1 = 0.0034$, $\nu_2 = -0.0874$, $\mu_2 = 0.004$, $n_2 = 0.1$ and $n_3 = -1$. (*a*): the real (solid) and imaginary (dashed) parts of the amplitude A, (*b*): the absolute value $|A|$, (*c*): the reconstructed solution $u = Ae^{ix} + \bar{A}e^{-ix}$, and (*d*): an approximation to the local wavenumber of the reconstructed solution in (*c*). The dashed lines correspond to $(k_-, k_+) = (0.946, 1.053)$.

5.1 *Interpretation of localized solutions via the amplitude equation*

The amplitude equation (3.5) has phase-winding solutions $A = Re^{iqX}$, with R and q related by (3.7). Previous work on this amplitude equation with $\nu_1 = 0$ (Gelens & Knobloch, 2009, 2010; Raitt & Riecke, 1995, 1997) – the complex Swift–Hohenberg equation with real coefficients – has identified solutions that are combinations of two phase-winding solutions with positive and negative values of q: these are precisely the localized patterns we found in the model PDE (2.5) and shown in Figure 6 (with $\nu_1 = f_1 + 2f_2 = 0$). Here we extend this interpretation to the case $\nu_1 \neq 0$.

In order to find localized solutions, we could develop a first integral and a Lyapunov function for (3.5) and look for pairs of solutions with the same values of the quantities. We reserve this for future work, and instead locate localized solutions of (3.5) by starting with a mixture of two phase-winding solutions with constituent wavenumbers q_- and q_+, and timestepping the PDE. Two examples are shown in Figures 8 (with $\nu_1 \neq 0$ and a small value of ν_2) and 9 (with $\nu_1 = 0$ and a larger value of ν_2).

Figure 8(*a*) shows the real (solid) and imaginary (dashed) parts of the solution A, $\Re(A)$ and $\Im(A)$ respectively. We can clearly see the transition from q_- to q_+ from $\Im(A)$, as the peaks of $\Im(A)$ shift from being on the right of the peaks of $\Re(A)$ to the left, and then back again. Figure 8(*b*) shows $|A|$, (half) the amplitude of the reconstructed pattern $u = Ae^{ix} + \bar{A}e^{-ix}$ shown in Figure 8(*c*). Figure 8(*d*) shows the approximation to the local wavenumber of the reconstructed pattern.

The example in Figure 9, with $\nu_1 = 0$, is similar, but shows more pronounced beating between the two wavenumbers, evident in the reconstructed solution and in Figure 6. The localized patterns found in the model PDE, with two wavenumbers, are thus interpreted in terms of combinations of phase-winding solutions of the complex Swift–Hohenberg equation, with positive and negative q. Kozyreff *et al.* (2009)

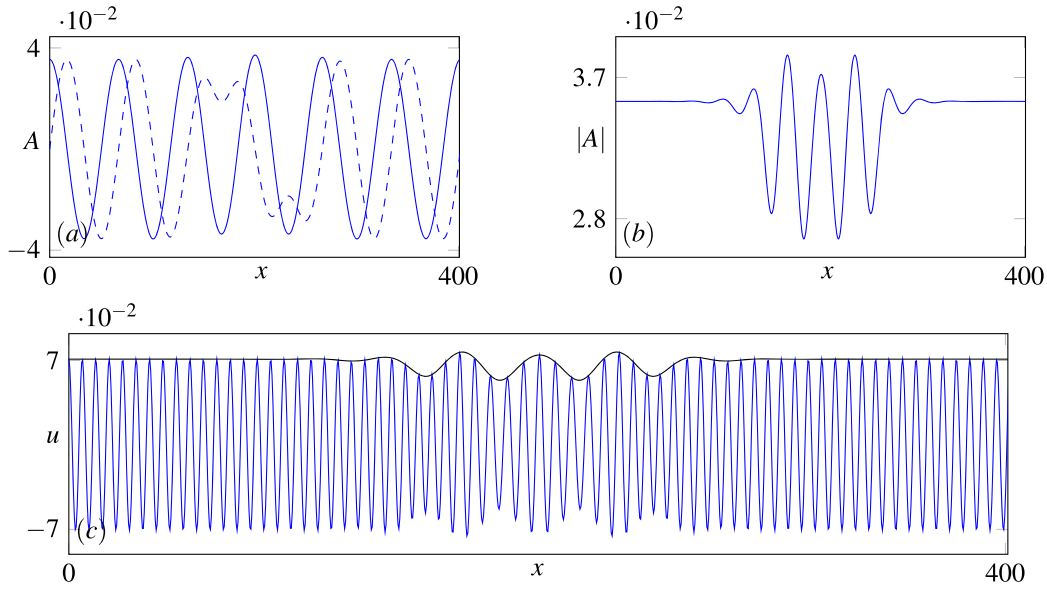

FIG. 9. Solution to (3.5), with $\nu_1 = 0$, $\nu_2 = -0.28$, $\mu_2 = 0.0025$, $n_2 = 0.1$ and $n_3 = -1$. (*a*): the real (solid) and imaginary (dashed) parts of the amplitude A, (*b*): the absolute value $|A|$, and (*c*): the reconstructed solution $u = Ae^{ix} + \bar{A}e^{-ix}$, with the amplitude $2|A|$ plotted also.

instead interpreted localized patches of patterns with two wavenumbers in terms of localized solutions of the real Swift–Hohenberg equation (1.1). We discuss this in more detail in §6.

5.2 *Addition of the Proctor term*

The branches of localized solutions shown in Figure 7 (without the Proctor term) do not close. We now investigate the addition of the Proctor term into the model, considering (2.4) with a rather large value of $\mu_p = -0.65$, chosen as to make the effects of this term more pronounced. We also fix $f_1 = 0.2814$ and $f_2 = -0.0721$ so that the marginal stability curve has two minima at different heights.

Seeking localized solutions, we plotted (as before) $\mathcal{H}$ and $\mathcal{F}$ (modified to include the Proctor term), looking for zero contours of $\mathcal{H}(k_+) - \mathcal{H}(k_-)$ and $\mathcal{F}(k_+) - \mathcal{F}(k_-)$, but we found no intersection of contours for the two minima at different heights for this choice of parameters. Notwithstanding this, we returned to wavenumbers $k_- = 58/64$ and $k_+ = 70/64$ and used a localized solution constructed from these constituent wavenumbers as a starting point for timestepping and continuation. Part of the resultant localized solution branch is shown in Figure 10. We see that including the Proctor term allows localized solutions of different widths on the same branch, rather than lying on distinct branches as in Figure 7. The existence of the localized solutions is also limited to a finite range of μ values; we expect the upper limit is introduced owing to the band of Eckhaus stable wavenumbers closing.

Figure 11 shows solutions at the saddle-nodes indicated in Figure 10. We notice that at each of these saddle-nodes the proportion of each pattern in the domain varies. Lower down the branch the pattern with the smaller wavenumber fills more of the domain, and conversely higher up the branch the pattern with the larger wavenumber fills more of the domain. This behaviour is qualitatively similar to the snaking behaviour of localized solutions in the subcritical Swift–Hohenberg equation (Burke &

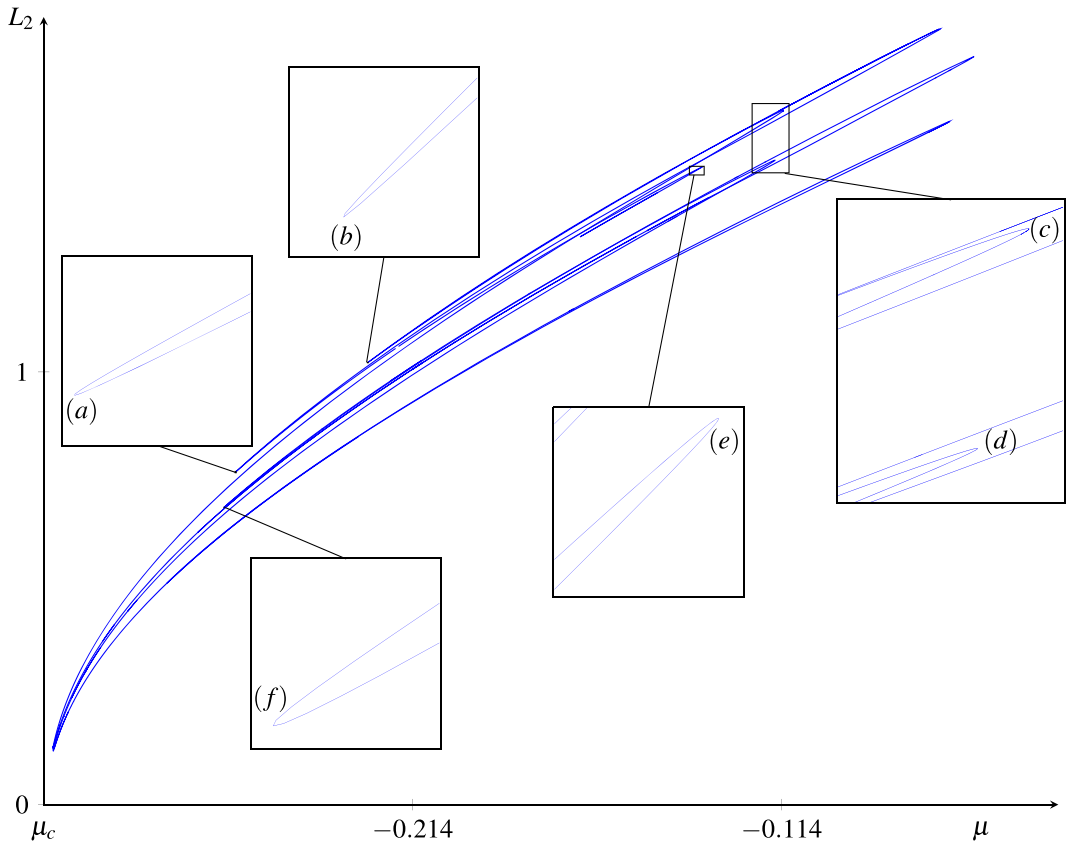

FIG. 10. Branch of localized solutions with $\mu_p = -0.65, f_1 = 0.2814, f_2 = -0.0721$. The critical value of the bifurcation parameter μ is $\mu_c = -0.314$. The interior saddle-nodes are magnified and the labels $(a) - (f)$ correspond to the solution profiles shown in Figure 11.

Knobloch, 2006), in that moving up the snaking branch adds to the width of the spatially periodic part of the localized solution—but the details, with saddle-node bifurcations appearing at many different places along the branch, are considerably more complicated, typical of snaking in more complicated situations such as hexagons (Lloyd *et al.*, 2008) or quasipatterns (Subramanian *et al.*, 2018) in two dimensions.

6. The Lugiato–Lefever and complex Swift–Hohenberg equations

As a related problem, we consider the Lugiato–Lefever equation

$$\frac{\partial \psi}{\partial t} = S - (1 + i\triangle)\,\psi + i|\psi|^2\psi - iB_2\frac{\partial^2 \psi}{\partial \tau^2} + iB_4\frac{\partial^4 \psi}{\partial \tau^4}, \tag{6.1}$$

which governs the envelope of the complex electromagnetic field $\psi(t, \tau)$ inside a photonic crystal fibre cavity (Tlidi *et al.*, 2007). In this equation, S represents an injected field, $\triangle$ is a cavity detuning, and B_2 and B_4 incorporate chromatic dispersion. The two time variables t and τ represent, respectively, the

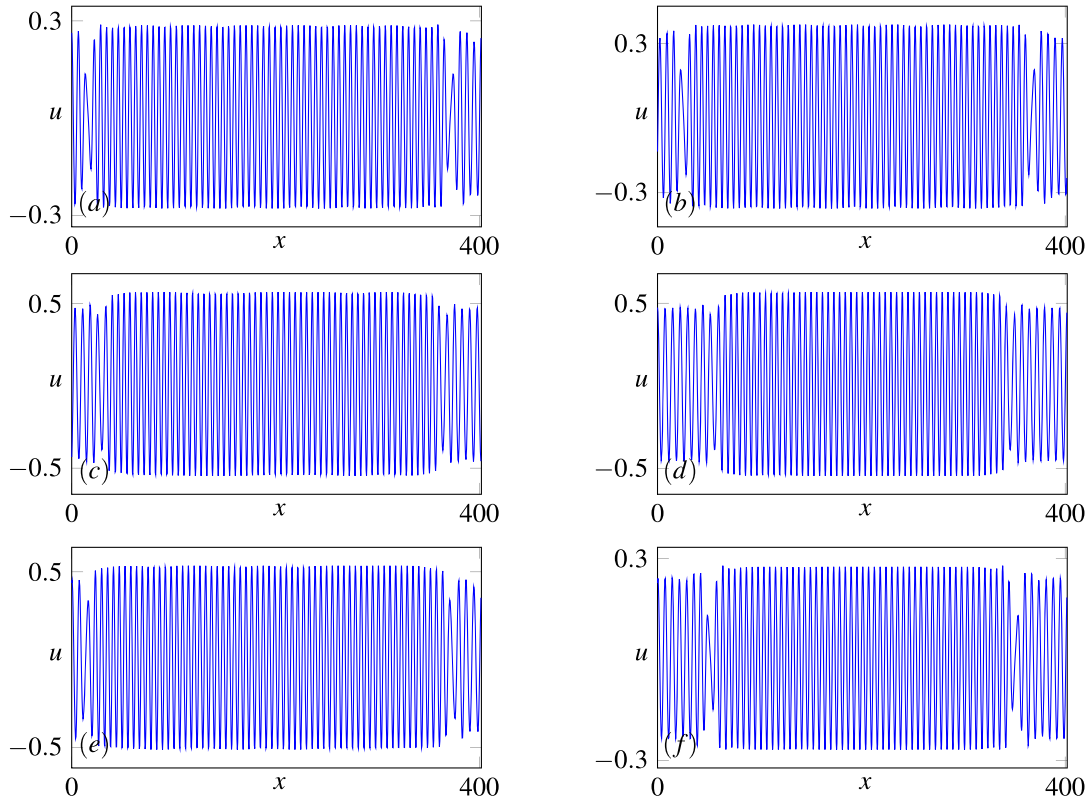

FIG. 11. Solutions at the saddle-nodes indicated in Figure 10.

average evolution of ψ over one cavity round trip and the fast variations of ψ. We note the similarities between (6.1) and (2.5): the independent variable τ is equivalent to x, there is a cubic nonlinearity, the inhomogeneous S term breaks the $\psi \to -\psi$ symmetry and implies a quadratic nonlinearity, and a fourth order complex equation is equivalent to an eighth order real equation.

This system also allows marginal stability curves with a double minimum, and Kozyreff *et al.* (2009) derived an amplitude equation similar to (3.5) for this case. Their analysis concentrates only on the case when the two minima occur at the same height, equivalent to $\gamma = 0$ in (3.2). This is a degenerate situation however; to recover the generic situation it is necessary to include a $B_3\partial^3\psi/\partial\tau^3$ term in (6.1). The degenerate case is chosen by Kozyreff *et al.* (2009) both as a means of simplifying the analysis and as a situation easily achievable experimentally.

With $\gamma = 0$, Bentley (2012) showed that the appropriate amplitude equation for the Lugiato–Lefever equation is (3.5) but with $\nu_1 = 0$. This special case is interesting: with $\nu_1 = 0$ and for $\nu_2 < 0$, equation (3.5) is equivalent to the *complex* Swift–Hohenberg equation:

$$\frac{\partial A}{\partial T} = \lambda A - \left(1 + \frac{\partial^2}{\partial X^2}\right)^2 A + n_A|A|^2 A, \tag{6.2}$$

having scaled and changed notation. This differs from the *real* SH equation (1.1) in that there is no quadratic term and that the cubic nonlinearity is $|A|^2A$ rather than u^3. It also differs from the more usual complex SH equation, which has complex coefficients (Sakaguchi, 1997). The complex SH equation with real coefficients has been investigated by Gelens & Knobloch (2010) and is equivalent to to the equation studied by Raitt & Riecke (1995). However, Kozyreff *et al.* (2009) found the real SH equation (1.1) as the amplitude equation for the Lugiato–Lefever problem, rather than the complex Swift–Hohenberg equation with real coefficients (6.2). This difference arises because effectively Kozyreff *et al.* (2009) took $u_1 = A(X,T)\cos(x)$ in (3.4) as the solution to the leading order linear equation, with real A. If instead they had taken $u_1 = A(X,T)e^{ix}+$c.c., with complex A, they would have recovered (6.2). As a result, we believe that the interpretation by Kozyreff *et al.* (2009) of localized solutions of (6.1) in terms of localized solutions of (1.1) should rather be done in terms of localized solutions of (6.2), which are different and have different stability properties. One feature not captured by localized solutions of (1.1) is the change in wavenumber between the different regions, as discussed in §5. The complex Swift–Hohenberg equation (6.2) does (since the coefficients are real) admit real solutions proportional to $\cos x$, but these solutions are unstable for the parameter values we tried. In addition, once the two minima have different heights, which would happen if the $B_3\partial^3\psi/\partial\tau^3$ term were included in the Lugiato–Lefever equation (6.1), then $u_1 = A(X,T)\cos x$ is not a viable starting point: equation (3.5) does not have real solutions when $\nu_1 \neq 0$.

7. Discussion and conclusions

The aim of this paper was to develop a new model equation (2.4) that captures qualitatively the behaviour of pattern-forming problems with a quartic marginal stability curve, and then explore the existence (and snaking) of localized solutions within this model equation. While we have focused on a particular example, we expect that the analysis could be extended to other models with a quartic marginal stability curve. There has been much progress in recent years developing a framework for the understanding of localized solutions in the Swift–Hohenberg equation (Dawes, 2010; Knobloch, 2015), where the existence of localized patterns is interpreted in terms of a stable pattern existing at the same parameter values as the stable trivial solution. Here we have shown that this scenario holds in the case of the unfolding of a quartic minimum, where there are coexisting stable patterns with two similar wavenumbers, and localized solutions consisting of combinations of these. This work fits in with other recent efforts that use Swift–Hohenberg-based (and other) models to explore problems with localization and snaking with multiple coexisting patterns (Alrihieli *et al.*, 2021; Knobloch *et al.*, 2019; Subramanian *et al.*, 2021).

We computed the weakly nonlinear amplitude equation for the model (2.5) and recovered a generalized Ginzburg–Landau equation (3.5). This allowed us to compute small-amplitude solutions with different wavelengths and to classify the Eckhaus stable patterns. Our work generalizes that of Raitt & Riecke (1995) and Gelens & Knobloch (2010), and corrects that of Kozyreff *et al.* (2009), to the case where the heights of the minima in the marginal stability curve are different. We made use of a first integral and a Lyapunov function to identify candidate initial conditions for finding localized solutions. Once the Proctor term, which allows the wavenumber of maximum growth rate to depend on the bifurcation parameter, is included in (2.4), the branches of localized solutions join up, but the snaking we find is considerably more complicated that the standard Swift–Hohenberg scenario.

An alternative approach to looking for localized solutions is to use spatial dynamics, seeking only steady solutions of the model equation. For the Swift–Hohenberg equation, this entails performing a normal form analysis of the Hamiltonian–Hopf bifurcation, which describes the bifurcation from the

basic state, and contains the familiar homoclinic snaking of localized solutions (Woods & Champneys, 1999). In this framework, the existence of localized solutions is determined by means of a geometric argument, whereby two integrals of the normal form define a space that can be divided into regions that allow or preclude the existence of localized solutions. In Appendix A, we derive a normal form for the bifurcation occurring at the quartic minimum of the model equation, following the derivation of the normal form for the Hamiltonian–Hopf bifurcation (Iooss & Adelmeyer, 1998; Woods & Champneys, 1999). We use two different methods (following Iooss & Adelmeyer (1998) and Burke & Knobloch (2007a)) to find the coefficients in the normal form. The two methods do not produce the same values for the coefficients in the normal form, and in either case, there were terms appearing in the normal form that one would have expected to be of higher order. As a consequence of these terms we were unable to find normal form integrals, including those one might expect by extension from the Hamiltonian–Hopf analysis. This means we can not employ a similar geometric analysis to find localized solutions. This normal form analysis merits further investigation. In particular, it would be interesting to ascertain the reasons for the difference between the normal form coefficients calculated by the two different methods, and also to determine whether any variant of the normal form is integrable: the variant we have derived does not seem to be.

Having found numerical localized solutions in the model equation, we could ask next whether examples more closely connected to reality might also have them, for example the magnetized Taylor–Couette system (Stefani *et al.*, 2009) and rotating magnetoconvection (Chandrasekhar, 1961; Cox & Matthews, 2001), where there are suggestions that marginal stability curves can change from having one to having two minima. This last example offers the interesting possibility of exploring two-dimensional patterns, potentially with regions of small hexagons embedded in a background of large hexagons, for example. This would be a natural extension to the study of localized solutions in (variants of) the two-dimensional Swift–Hohenberg equation (Lloyd *et al.*, 2008; Subramanian *et al.*, 2018, 2021), in systems with parametric driving like the Faraday wave experiment (Alnahdi *et al.*, 2018; Arbell & Fineberg, 2000), and in reaction–diffusion systems (Tlidi *et al.*, 2012).

The coalescence of the two minima is in itself an interesting problem. In one-dimensional systems with marginal stability curves with two minima far apart, the natural approach is to reduce the problem to two coupled second-order Ginzburg–Landau equations (Dawes & Proctor, 2008), and there are model equations based on the Swift–Hohenberg equation that allow pattern formation on two length scales (Lifshitz & Petrich, 1997; Müller, 1994; Rucklidge *et al.*, 2012). It would thus be interesting to investigate how one would transition from the situation of two well separated length scales to the unfolding of a quartic minimum, in one or more dimensions.

Acknowledgements

Thomas Wagenknecht (1974–2012) co-supervised much of the work presented in this paper: DCB and AMR gratefully acknowledge his perceptive insight and infectious enthusiasm. This project was inspired by conversations with Rainer Hollerbach. We also acknowledge useful discussions and correspondence with Jonathan Dawes, Gérard Iooss, Edgar Knobloch, Gregory Kozyreff, Eric Lombardi, Michael Proctor and Priya Subramanian. This research was supported by a PhD studentship from the Science and Technology Facilities Council (STFC).

References

Alnahdi, A., Niesen, J. & Rucklidge, A. M. (2018) Localized patterns in periodically forced systems: II. Patterns with nonzero wavenumber. *SIAM J. Appl. Dynam. Syst.*, **17**, 1478–1502.

Alrihieli, H., Rucklidge, A. M. & Subramanian, P. (2021) Spatial localization beyond steady states in the neighbourhood of the Takens–Bogdanov bifurcation. *IMA J. Appl. Math.*, in press.

Arbell, H. & Fineberg, J. (2000) Temporally harmonic oscillons in Newtonian fluids. *Phys. Rev. Lett.*, **85**, 756–759.

Beck, M., Knobloch, J., Lloyd, D. J., Sandstede, B. & Wagenknecht, T. (2009) Snakes, ladders, and isolas of localized patterns. *SIAM J. Math. Anal.*, **41**, 936–972.

Bentley, D. C. (2012) *Localised solutions in the magnetorotational Taylor–Couette flow with a quartic marginal stability curve*, Ph.D. Thesis. University of Leeds.

Bortolozzo, U., Clerc, M. G., Falcon, C., Residori, S. & Rojas, R. (2006) Localized states in bistable pattern-forming systems. *Phys. Rev. Lett.*, **96**, 214501.

Burke, J. & Dawes, J. H. P. (2012) Localized states in an extended Swift–Hohenberg equation. *SIAM J. Appl. Dyn. Syst.*, **11**, 261–284.

Burke, J. & Knobloch, E. (2006) Localized states in the generalized Swift–Hohenberg equation. *Phys. Rev. E*, **73**, 056211.

Burke, J. & Knobloch, E. (2007a) Normal form for spatial dynamics in the Swift–Hohenberg equation. *Discrete Contin. Dyn. Sys. Suppl.*, **2007**, 170–180.

Burke, J. & Knobloch, E. (2007b) Snakes and ladders: localized states in the Swift–Hohenberg equation. *Phys. Lett. A*, **360**, 681–688.

Castelino, J. K., Ratliff, D. J., Rucklidge, A. M., Subramanian, P. & Topaz, C. M. (2020) Spatiotemporal chaos and quasipatterns in coupled reaction–diffusion systems. *Phys. D*, **407**, 132475.

Chandrasekhar, S. (1961) *Hydrodynamic and Hydromagnetic Stability*. Oxford: Clarendon Press.

Chapman, S. J. & Kozyreff, G. (2009) Exponential asymptotics of localised patterns and snaking bifurcation diagrams. *Phys. D*, **238**, 319–354.

Coullet, P., Riera, C. & Tresser, C. (2000) Stable static localized structures in one dimension. *Phys. Rev. Lett.*, **84**, 3069–3072.

Cox, S. M. & Matthews, P. C. (2001) New instabilities in two-dimensional rotating convection and magnetoconvection. *Phys. D*, **149**, 210–229.

Cox, S. M. & Matthews, P. C. (2002) Exponential time differencing for stiff systems. *J. Comp. Phys.*, **176**, 430–455.

Crawford, C. & Riecke, H. (1999) Oscillon-type structures and their interaction in a Swift–Hohenberg model. *Phys. D*, **129**, 83–92.

Cross, M. C. & Hohenberg, P. C. (1993) Pattern formation outside of equilibrium. *Rev. Modern Phys.*, **65**, 851–1112.

Dawes, J. H. P. (2010) The emergence of a coherent structure for coherent structures: localized states in nonlinear systems. *Phil. Trans. Roy. Soc. A*, **368**, 3519–3534.

Dawes, J. H. P. & Proctor, M. R. E. (2008) Secondary Turing-type instabilities due to strong spatial resonance. *Proc. Roy. Soc. A*, **464**, 923–942.

Doedel, E. J. (2007) AUTO07p: continuation and bifurcation software for ordinary differential equations. *Technical Report*. Montreal: Concordia University.

Eckhaus, W. (1965) *Studies in Nonlinear Stability Theory*. Berlin: Springer-Verlag.

Edwards, W. S. & Fauve, S. (1994) Patterns and quasi-patterns in the Faraday experiment. *J. Fluid Mech.*, **278**, 123–148.

Elphick, C., Tirapegui, E., Brachet, M. E., Coullet, P. & Iooss, G. (1987) A simple global characterization for normal forms of singular vector fields. *Phys. D*, **29**, 95–127.

Gelens, L. & Knobloch, E. (2009) Faceting and coarsening dynamics in the complex Swift–Hohenberg equation. *Phys. Rev. E*, **80**, 0462201.

GELENS, L. & KNOBLOCH, E. (2010) Coarsening and frozen faceted structures in the complex Swift–Hohenberg equation. *Eur. Phys. J. D*, **59**, 23–36.

HARAGUS, M. & IOOSS, G. (2011) *Local Bifurcations, Center Manifolds, and Normal Forms in Infinite Dimensional Systems*. London: Springer.

HEGSETH, J., VINCE, J. M., DUBOIS, M. & BERGE, M. (1992) Pattern domains in Rayleigh–Bénard slot convection. *Europhys. Lett.*, **17**, 413–418.

HILALI, M. F., MÉTENS, S., BORCKMANS, P. & DEWEL, G. (1995) Pattern selection in the generalized Swift–Hohenberg model. *Phys. Rev. E*, **51**, 2046–2052.

HOLL, M. P., ARCHER, A. J. & THIELE, U. (2021) Efficient calculation of phase coexistence and phase diagrams: application to a binary phase-field crystal model. *J. Phys.: Condens. Matter*, **33**, 115401.

HOYLE, R. B. (2006) *Pattern Formation: An Introduction to Methods*. Cambridge: Cambridge University Press.

IOOSS, G. & ADELMEYER, M. (1998) *Topics in Bifurcation Theory and Applications. Advanced Series in Nonlinear Dynamics, vol. 3*, 2nd edn. Singapore: World Scientific Publishing Co., Inc.

IOOSS, G. & PÉROUÈME, M. C. (1993) Perturbed homoclinic solutions in reversible 1:1 resonance vector fields. *J. Diff. Eq.*, **102**, 62–88.

KNOBLOCH, E. (1990) Pattern selection in long-wavelength convection. *Phys. D*, **41**, 450–479.

KNOBLOCH, E. (2015) Spatial localization in dissipative systems. *Annu. Rev. Condens. Matter Phys.*, **6**, 325–359.

KNOBLOCH, E., UECKER, H. & WETZEL, D. (2019) Defectlike structures and localized patterns in the cubic-quintic-septic Swift–Hohenberg equation. *Phys. Rev. E*, **100**, 012204.

KOZYREFF, G., TLIDI, M., MUSSOT, A., LOUVERGNEAUX, E., TAKI, M. & VLADIMIROV, A. G. (2009) Localized beating between dynamically generated frequencies. *Phys. Rev. Lett.*, **102**, 043905.

KOZYREFF, G. & CHAPMAN, S. J. (2006) Asymptotics of large bound states of localized structures. *Phys. Rev. Lett.*, **97**, 044502.

LIFSHITZ, R. & PETRICH, D. M. (1997) Theoretical model for Faraday waves with multiple-frequency forcing. *Phys. Rev. Lett.*, **79**, 1261–1264.

LLOYD, D. J. B., SANDSTEDE, B., AVITABILE, D. & CHAMPNEYS, A. R. (2008) Localized hexagon patterns of the planar Swift–Hohenberg equation. *SIAM J. Appl. Dynam. Syst.*, **7**, 1049–1100.

MAMATSASHVILI, G., STEFANI, F., HOLLERBACH, R. & RÜDIGER, G. (2019) Two types of axisymmetric helical magnetorotational instability in rotating flows with positive shear. *Phys. Rev. Fluids*, **4**, 103905.

MÜLLER, H. W. (1994) Model equations for two-dimensional quasipatterns. *Phys. Rev. E*, **49**, 1273–1277.

MURDOCK, J. (2003) *Normal Forms and Unfoldings for Local Dynamical Systems*. New York: Springer-Verlag.

POMEAU, Y. (1986) Front motion, metastability and subcritical bifurcations in hydrodynamics. *Phys. D*, **23**, 3–11.

PROCTOR, M. R. E. (1991) Instabilities of roll-like patterns for degenerate marginal curves. *Phys. Fluids*, **3**, 299–302.

RAITT, D. & RIECKE, H. (1995) Domain structures in fourth-order phase and Ginzburg–Landau equations. *Phys. D*, **82**, 79–94.

RAITT, D. & RIECKE, H. (1997) Parametric forcing of waves with non-monotonic dispersion relation: domain structures in ferrofluids. *Phys. Rev. E*, **55**, 5448–5454.

REES, D. A. S. & MOJTABI, A. (2013) The effect of conducting boundaries on Lapwood–Prats convection. *Int. J. Heat Mass Transfer*, **65**, 765–778.

RIECKE, H. (1990) Stable wave-number kinks in parametrically excited standing waves. *Europhys. Lett. (EPL)*, **11**, 213–218.

RILEY, D. S. & DAVIS, S. H. (1989) Eckhaus instabilities in generalized Landau–Ginzburg equations. *Phys. Fluids A*, **1**, 1745–1747.

RUCKLIDGE, A. M., SILBER, M. & SKELDON, A. C. (2012) Three-wave interactions and spatiotemporal chaos. *Phys. Rev. Lett.*, **108**, 074504.

RUCKLIDGE, A. M. & SILBER, M. (2009) Design of parametrically forced patterns and quasipatterns. *SIAM J. Appl. Dynam. Syst.*, **8**, 298–347.

SAKAGUCHI, H. (1997) Standing wave patterns for the complex Swift–Hohenberg equation. *Prog. Theor. Phys.*, **98**, 577–585.

Skeldon, A. C. & Rucklidge, A. M. (2015) Can weakly nonlinear theory explain Faraday wave patterns near onset? *J. Fluid Mech.*, **777**, 604–632.

Spina, A., Toomre, J. & Knobloch, E. (1998) Confined states in large-aspect-ratio thermosolutal convection. *Phys. Rev. E*, **57**, 524–545.

Stefani, F., Gerbeth, G., Gundrum, T., Hollerbach, R., Priede, J., Rüdiger, G. & Szklarski, J. (2009) Helical magnetorotational instability in a Taylor–Couette flow with strongly reduced Ekman pumping. *Phys. Rev. E*, **80**, 066303.

Subramanian, P., Archer, A. J., Knobloch, E. & Rucklidge, A. M. (2018) Spatially localized quasicrystalline structures. *New J. Phys.*, **20**, 122002.

Subramanian, P., Archer, A. J., Knobloch, E. & Rucklidge, A. M. (2021) Snaking without subcriticality: grain boundaries as non-topological defects. *IMA J. Appl. Math.*, in press.

Swift, J. & Hohenberg, P. C. (1977) Hydrodynamic fluctuations at the convective instability. *Phys. Rev. A*, **15**, 319–328.

Tlidi, M., Mussot, A., Louvergneaux, E., Kozyreff, G., Vladimirov, A. G. & Taki, M. (2007) Control and removal of modulational instabilities in low-dispersion photonic crystal fiber cavities. *Opt. Lett.*, **32**, 662–664.

Tlidi, M., Sonnino, G. & Bachir, M. (2012) Predicted formation of localized superlattices in spatially distributed reaction-diffusion solutions. *Phys. Rev. E*, **86**, 045103.

Topaz, C. M. & Silber, M. (2002) Resonances and superlattice pattern stabilization in two-frequency forced Faraday waves. *Phys. D*, **172**, 1–29.

Woods, P. D. & Champneys, A. R. (1999) Heteroclinic tangles and homoclinic snaking in the unfolding of a degenerate reversible Hamiltonian–Hopf bifurcation. *Phys. D*, **129**, 147–170.

A. A normal form for the model equation

In this Appendix we derive the normal form for the model equation, with the intention of extending the analysis of the Hamiltonian–Hopf bifurcation in the Swift–Hohenberg equation (Iooss & Pérouème, 1993; Woods & Champneys, 1999) to this case of quadruply degenerate eigenvalues. Our approach is based on that of these authors (see also Haragus & Iooss (2011)), along with the work of Burke & Knobloch (2007a). For additional details of the calculations in this Appendix, see Bentley (2012).

In general, we consider dynamical systems of the form

$$\frac{d\mathbf{z}}{dx} = F(\mathbf{z}, \boldsymbol{\varrho}), \qquad \mathbf{z} \in \mathbb{R}^n, \qquad \boldsymbol{\varrho} \in \mathbb{R}^m, \tag{A.1}$$

where we assume that

$$F(0,0) = 0,$$

and also that there is a symmetry $\mathcal{R}$ such that

$$F(\mathcal{R}\mathbf{z}, \boldsymbol{\varrho}) = -\mathcal{R}F(\mathbf{z}, \boldsymbol{\varrho}).$$

This symmetry $\mathcal{R}$ is known as a reversibility symmetry. We consider reversible systems because of the invariance of the model equation (2.5) under spatial reversibility $x \to -x$. The parameter vector $\boldsymbol{\varrho} = 0$ is chosen so that the eigenvalues of the $\mathbf{z} = 0$ equilibrium are all on the imaginary axis.

We aim to derive the normal form of the model equation near the bifurcation This derivation essentially entails finding a near-identity transform

$$\mathbf{z} \to \tilde{\mathbf{z}} + \boldsymbol{\Phi}(\tilde{\mathbf{z}}, \boldsymbol{\varrho}),$$

such that we may write (A.1) in the form

$$\frac{d\tilde{\mathbf{z}}}{dx} = L_0\tilde{\mathbf{z}} + \mathbf{P}(\tilde{\mathbf{z}}, \boldsymbol{\varrho}) + o((||\tilde{\mathbf{z}}|| + ||\boldsymbol{\varrho}||)^{k_p}). \tag{A.2}$$

Here $\boldsymbol{\Phi}(\tilde{\mathbf{z}}, \boldsymbol{\varrho})$ and $\mathbf{P}(\tilde{\mathbf{z}}, \boldsymbol{\varrho})$ are (n-dimensional vectors of) polynomials of degree $\leq k_p$, and L_0 is a constant coefficient matrix in Jordan normal form. The polynomial $\mathbf{P}$ satisfies the so-called homological equation

$$\mathbf{P}\left(e^{xL_0^*}\tilde{\mathbf{z}}, \boldsymbol{\varrho}\right) = e^{xL_0^*}\mathbf{P}\left(\tilde{\mathbf{z}}, \boldsymbol{\varrho}\right) \qquad \forall\, \tilde{\mathbf{z}}, \boldsymbol{\varrho} \text{ and } x,$$

where L_0^* is the adjoint (conjugate transpose) of L_0. An equivalent statement is found by differentiating the equation with respect to x and evaluating at $x = 0$, which gives

$$\tilde{D}\mathbf{P}\left(\tilde{\mathbf{z}}, \boldsymbol{\varrho}\right) L_0^*\tilde{\mathbf{z}} = L_0^*\mathbf{P}\left(\tilde{\mathbf{z}}, \boldsymbol{\varrho}\right) \qquad \forall\, \tilde{\mathbf{z}} \text{ and } \boldsymbol{\varrho},$$

where $\tilde{D}\mathbf{P}\left(\tilde{\mathbf{z}}, \boldsymbol{\varrho}\right)$ is the Jacobian matrix of $\mathbf{P}$.

There is some freedom in determining the polynomial $\mathbf{P}$; the idea is to choose $\mathbf{P}$ to be as simple as possible. Of course, this freedom means that there is not a unique normal form. Rather, the choice of $\mathbf{P}$ is known as the style of the normal form. The two main styles are the inner-product style popularized by Elphick *et al.* (1987) and the $sl(2)$ style popularized by Cushman and Sanders (Murdock, 2003). We will use the inner-product style, since this style is used for the Hamiltonian–Hopf bifurcation (Iooss

& Adelmeyer, 1998), which describes the bifurcation from the basic state in the Swift–Hohenberg equation.

In what follows, we will derive the normal form at the codimension 3 point $\mu = f_1 = f_2 = 0$, which corresponds to $\boldsymbol{\varrho} = 0$ in (A.1). So, the homological equation we will actually use is

$$\tilde{D}\mathbf{P}\left(\tilde{\mathbf{z}}\right) L_0^* \tilde{\mathbf{z}} = L_0^* \mathbf{P}\left(\tilde{\mathbf{z}}\right) \qquad \forall\, \tilde{\mathbf{z}}. \tag{A.3}$$

The parameters μ, f_1 and f_2 can be added in as unfoldings once the normal form has been found.

A.1 *Linear part of the normal form*

In this section, we write the dynamical system describing steady solutions of the model equation. We then determine the linear part of the coordinate transformation $\mathbf{z} \to \tilde{\mathbf{z}}$. By considering steady solutions of our model equation (2.5) with $\mu = f_1 = f_2 = 0$, *i.e.*, solutions of

$$0 = -\left(1 + \frac{\partial^2}{\partial x^2}\right)^4 u + n_2 u^2 + n_3 u^3, \tag{A.4}$$

we can convert (A.4) into a system of eight first-order ODEs, such that we have the appropriate form (A.1). To do this, we introduce new variables

$$z_1 = u, \qquad z_2 = u_x, \qquad z_3 = u_{xx}, \qquad \ldots, \qquad z_8 = u_{xxxxxx},$$

and write

$$\frac{d\mathbf{z}}{dx} = F(\mathbf{z}) = L_0\mathbf{z} + N(\mathbf{z}), \tag{A.5}$$

where $\mathbf{z} = (z_1, z_2, z_3, z_4, z_5, z_6, z_7, z_8)^T$. The linear and nonlinear parts of (A.5) are given by

$$L_0 = \begin{pmatrix} 0 & 1 & 0 & 0 & 0 & 0 & 0 & 0 \\ 0 & 0 & 1 & 0 & 0 & 0 & 0 & 0 \\ 0 & 0 & 0 & 1 & 0 & 0 & 0 & 0 \\ 0 & 0 & 0 & 0 & 1 & 0 & 0 & 0 \\ 0 & 0 & 0 & 0 & 0 & 1 & 0 & 0 \\ 0 & 0 & 0 & 0 & 0 & 0 & 1 & 0 \\ 0 & 0 & 0 & 0 & 0 & 0 & 0 & 1 \\ -1 & 0 & -4 & 0 & -6 & 0 & -4 & 0 \end{pmatrix} \quad \text{and} \quad N(\mathbf{z}) = \begin{pmatrix} 0 \\ 0 \\ 0 \\ 0 \\ 0 \\ 0 \\ 0 \\ n_2 z_1^2 + n_3 z_1^3 \end{pmatrix}.$$

The reversibility $\mathcal{R}$ acting on the elements of $\mathbf{z}$ is defined as $\mathcal{R}z_i = (-1)^{i-1} z_i$ for $i = 1, \ldots, 8$.

The first step is to transform L_0 into Jordan normal form. The eigenvalues are $\lambda_\pm = \pm i$ with algebraic multiplicity 4 and geometric multiplicity 1, so each eigenvalue has one eigenvector and three

generalized eigenvectors. These are readily found:

$$\boldsymbol{\zeta}_0 = \begin{pmatrix} 1 \\ i \\ -1 \\ -i \\ 1 \\ i \\ -1 \\ -i \end{pmatrix}, \qquad \boldsymbol{\zeta}_1 = \begin{pmatrix} 0 \\ 1 \\ 2i \\ -3 \\ -4i \\ 5 \\ 6i \\ -7 \end{pmatrix}, \qquad \boldsymbol{\zeta}_2 = \begin{pmatrix} 0 \\ 0 \\ 1 \\ 3i \\ -6 \\ -10i \\ 15 \\ 21i \end{pmatrix}, \qquad \boldsymbol{\zeta}_3 = \begin{pmatrix} 0 \\ 0 \\ 0 \\ 1 \\ 4i \\ -10 \\ -20i \\ 35 \end{pmatrix}, \tag{A.6}$$

with $L\boldsymbol{\zeta}_0 = \lambda_+\boldsymbol{\zeta}_0$ and $L\boldsymbol{\zeta}_j = \lambda_+\boldsymbol{\zeta}_j + \boldsymbol{\zeta}_{j-1}$, with $j = 1, 2, 3$. We now define the linear transformation

$$\mathbf{z} = \boldsymbol{\zeta}_0 A + \boldsymbol{\zeta}_1 B + \boldsymbol{\zeta}_2 C + \boldsymbol{\zeta}_3 D + \bar{\boldsymbol{\zeta}}_0 \bar{A} + \bar{\boldsymbol{\zeta}}_1 \bar{B} + \bar{\boldsymbol{\zeta}}_2 \bar{C} + \bar{\boldsymbol{\zeta}}_3 \bar{D}, \tag{A.7}$$

where the overbar denotes complex conjugation, and A, B, C and D are complex functions of x. The transformed linear normal form is $\frac{d\tilde{\mathbf{z}}}{dx} = L_0\tilde{\mathbf{z}}$, where the transformed L_0 and its adjoint L_0^* are

$$L_0 = \begin{pmatrix} i & 1 & 0 & 0 & 0 & 0 & 0 & 0 \\ 0 & i & 1 & 0 & 0 & 0 & 0 & 0 \\ 0 & 0 & i & 1 & 0 & 0 & 0 & 0 \\ 0 & 0 & 0 & i & 0 & 0 & 0 & 0 \\ 0 & 0 & 0 & 0 & -i & 1 & 0 & 0 \\ 0 & 0 & 0 & 0 & 0 & -i & 1 & 0 \\ 0 & 0 & 0 & 0 & 0 & 0 & -i & 1 \\ 0 & 0 & 0 & 0 & 0 & 0 & 0 & -i \end{pmatrix} \quad \text{and} \quad L_0^* = \begin{pmatrix} -i & 0 & 0 & 0 & 0 & 0 & 0 & 0 \\ 1 & -i & 0 & 0 & 0 & 0 & 0 & 0 \\ 0 & 1 & -i & 0 & 0 & 0 & 0 & 0 \\ 0 & 0 & 1 & -i & 0 & 0 & 0 & 0 \\ 0 & 0 & 0 & 0 & i & 0 & 0 & 0 \\ 0 & 0 & 0 & 0 & 1 & i & 0 & 0 \\ 0 & 0 & 0 & 0 & 0 & 1 & i & 0 \\ 0 & 0 & 0 & 0 & 0 & 0 & 1 & i \end{pmatrix}.$$

Thus, the linear part of the normal form is

$$\frac{dA}{dx} = iA + B, \qquad \frac{dB}{dx} = iB + C, \qquad \frac{dC}{dx} = iC + D, \qquad \frac{dD}{dx} = iD. \tag{A.8}$$

along with the complex conjugates of these.

A.2 *Nonlinear part of the normal form*

To determine the nonlinear part of the normal form $\mathbf{P}(\tilde{\mathbf{z}})$ we make use of the homological equation (A.3). We truncate at cubic order, setting $k_p = 3$ in (A.2). We also take in to account the linear transformation in §A.1, now thinking of $\tilde{\mathbf{z}}$ as $(A, B, C, D, \bar{A}, \bar{B}, \bar{C}, \bar{D})$.

One possible approach to determining the nonlinear part of the normal form is to suppose $\mathbf{P}(\tilde{\mathbf{z}})$ contains all possible quadratic and cubic combinations of the components of $\tilde{\mathbf{z}}$, *i.e.*,

$$\mathbf{P}(\tilde{\mathbf{z}}) = \sum_{i,j,k,l,m,n,o,p=0}^{3} \boldsymbol{\Gamma}_{ijklmnop} A^i B^j C^k D^l \bar{A}^m \bar{B}^n \bar{C}^o \bar{D}^p,$$

such that $i+j+k+l+m+n+o+p = 2$ or 3. Then, plugging this into the homological equation (A.3) gives the terms and the combinations in which they must appear. This allows us to write the normal

form as:

$$\begin{aligned}\frac{dA}{dx} = {} & iA + B + \gamma_1|A|^2A + \gamma_2A\left(A\bar{B} - \bar{A}B\right) + \gamma_3A\left(A\bar{C} - |B|^2 + \bar{A}C\right) \\ & + \gamma_4A\left(A\bar{D} - B\bar{C} + \bar{B}C - \bar{A}D\right) + \gamma_5\bar{A}\left(B^2 - 2AC\right) \\ & + 3\gamma_6\left(\bar{B}\left(B^2 - 2AC\right) + \bar{A}\left(3AD - BC\right)\right),\end{aligned} \tag{A.9a}$$

$$\begin{aligned}\frac{dB}{dx} = {} & iB + C + \gamma_1|A|^2B + \gamma_2B\left(A\bar{B} - \bar{A}B\right) + \gamma_3B\left(A\bar{C} - |B|^2 + \bar{A}C\right) \\ & + \gamma_4B\left(A\bar{D} - B\bar{C} + \bar{B}C - \bar{A}D\right) + \gamma_5\bar{B}\left(B^2 - 2AC\right) \\ & + \gamma_6\left(2\bar{A}\left(3BD - 2C^2\right) + \bar{B}\left(3AD - BC\right) + 4\bar{C}\left(B^2 - 2AC\right)\right) \\ & + \gamma_7|A|^2A + \gamma_8A\left(A\bar{B} - \bar{A}B\right) + \gamma_9A\left(A\bar{C} - |B|^2 + \bar{A}C\right) \\ & + \gamma_{10}A\left(A\bar{D} - B\bar{C} + \bar{B}C - \bar{A}D\right) + 2\gamma_{11}\bar{A}\left(B^2 - 2AC\right) \\ & + \gamma_{12}\left(\bar{B}\left(B^2 - 2AC\right) + \bar{A}\left(3AD - BC\right)\right),\end{aligned} \tag{A.9b}$$

$$\begin{aligned}\frac{dC}{dx} = {} & iC + D + \gamma_1|A|^2C + \gamma_2C\left(A\bar{B} - \bar{A}B\right) + \gamma_3C\left(A\bar{C} - |B|^2 + \bar{A}C\right) \\ & + \gamma_4C\left(A\bar{D} - B\bar{C} + \bar{B}C - \bar{A}D\right) + \gamma_5\bar{C}\left(B^2 - 2AC\right) \\ & + \gamma_6\left(2\bar{B}\left(3BD - 2C^2\right) - \bar{C}\left(3AD - BC\right) + 3\bar{D}\left(B^2 - 2AC\right)\right) \\ & + \gamma_7|A|^2B + \gamma_8B\left(A\bar{B} - \bar{A}B\right) + \gamma_9B\left(A\bar{C} - |B|^2 + \bar{A}C\right) \\ & + \gamma_{10}B\left(A\bar{D} - B\bar{C} + \bar{B}C - \bar{A}D\right) + \gamma_{11}\left(\bar{B}\left(B^2 - 2AC\right) - \bar{A}\left(3AD - BC\right)\right) \\ & + \gamma_{12}\left(2\bar{B}\left(3AD - BC\right) + 3\bar{C}\left(B^2 - 2AC\right) - \bar{A}\left(3BD - 2C^2\right)\right) + \gamma_{13}|A|^2A \\ & + \gamma_{14}A\left(A\bar{B} - \bar{A}B\right) + \gamma_{15}A\left(A\bar{C} - |B|^2 + \bar{A}C\right) \\ & + \gamma_{16}A\left(A\bar{D} - B\bar{C} + \bar{B}C - \bar{A}D\right) + \gamma_{17}\bar{A}\left(B^2 - 2AC\right) + \gamma_{18}\left(\bar{A}\left(3BD - 2C^2\right)\right. \\ & \left. - \bar{B}\left(3AD - BC\right) - \bar{C}\left(B^2 - 2AC\right)\right) + \gamma_{19}\left(\bar{B}\left(B^2 - 2AC\right) + \bar{A}\left(3AD - BC\right)\right),\end{aligned} \tag{A.9c}$$

$$\begin{aligned}\frac{dD}{dx} = {} & iD + \gamma_1|A|^2D + \gamma_2 D\left(A\bar{B} - \bar{A}B\right) + \gamma_3 D\left(A\bar{C} - |B|^2 + \bar{A}C\right) \\ & + \gamma_4 D\left(A\bar{D} - B\bar{C} + \bar{B}C - \bar{A}D\right) + \gamma_5\bar{D}\left(B^2 - 2AC\right) \\ & + \gamma_6\left(2\bar{C}\left(3BD - 2C^2\right) - 3\bar{D}\left(3AD - BC\right)\right) + \gamma_7|A|^2C \\ & + \gamma_8 C\left(A\bar{B} - \bar{A}B\right) + \gamma_9 C\left(A\bar{C} - |B|^2 + \bar{A}C\right) + \gamma_{10}C\left(A\bar{D} - B\bar{C} + \bar{B}C - \bar{A}D\right) \\ & - \gamma_{11}\bar{B}\left(3AD - BC\right) + \gamma_{12}\left(3\bar{C}\left(B^2 - 2AC\right) + 6\bar{D}\left(3AD - BC\right)\right. \\ & \quad \left. - \bar{B}\left(3BD - 2C^2\right)\right) + \gamma_{13}|A|^2B + \gamma_{14}B\left(A\bar{B} - \bar{A}B\right) + \gamma_{15}B\left(A\bar{C} - |B|^2 + \bar{A}C\right) \\ & - \gamma_{17}\bar{A}\left(3AD - BC\right) + \gamma_{18}\left(\bar{B}\left(3BD - 2C^2\right) - 2\bar{C}\left(B^2 - 2AC\right)\right. \\ & \quad \left. - 3\bar{D}\left(3AD - BC\right)\right) + \gamma_{19}\left(2\bar{A}\left(3BD - 2C^2\right) - \bar{B}\left(3AD - BC\right)\right) \\ & + \gamma_{20}|A|^2A + \gamma_{21}A\left(A\bar{B} - \bar{A}B\right) + \gamma_{22}A\left(A\bar{C} - |B|^2 + \bar{A}C\right) \\ & + \gamma_{23}A\left(A\bar{D} - B\bar{C} + \bar{B}C - \bar{A}D\right) + \gamma_{24}\bar{A}\left(B^2 - 2AC\right) + \gamma_{25}\left(\bar{B}\left(3AD - BC\right)\right. \\ & \quad \left. - \bar{A}\left(3BD - 2C^2\right) + \bar{C}\left(B^2 - 2AC\right)\right) + \gamma_{26}\left(\bar{A}\left(3AD - BC\right)\right. \\ & \quad \left. + \bar{B}\left(B^2 - 2AC\right)\right), \end{aligned} \tag{A.9d}$$

where the coefficients γ_i, $i = 1, \ldots, 26$ are to be determined by transforming the nonlinear term $n_2u^2 + n_3u^3$. One may notice that (A.9) contains no quadratic terms; the requirement that we satisfy the homological equation (A.3) excludes them. Had we chosen a different normal form style, *e.g.*, the $sl(2)$ style (Murdock, 2003), then it is possible that (A.9) would have contained quadratic terms.

An alternative approach to constructing the normal form is to find first integrals of the homological equation and construct the polynomials $\mathbf{P}(\tilde{\mathbf{z}})$ using these, following Elphick *et al.* (1987). For details, see Bentley (2012). The end result is a set of first integrals $c_1, \ldots, c_7$, given in Table A.1. Note that c_2, c_4 and c_6 contain $\log(A)$, so we also use w_1 and w_2, which are combinations of the first seven with the $\log(A)$ dependence eliminated. We note that the integrals c_1, c_2 and c_3 are also integrals of the characteristic system in the four-dimensional Hamiltonian–Hopf case (Iooss & Adelmeyer, 1998).

From the first integrals of the homological equation, we can construct the nonlinear part of the normal form. We make the change of variables

$$(A, B, C, D, \bar{A}, \bar{B}, \bar{C}, \bar{D}) \to (A, c_1, c_2, c_3, c_5, c_7, w_1, w_2),$$

and solve the homological equation in these new variables (see Bentley, 2012), giving, for the first equation in the normal form:

$$\frac{dA}{dx} = iA + B + P_1(A, B, C, D, \bar{A}, \bar{B}, \bar{C}, \bar{D}) = iA + B + A\varphi(c_1, c_2, c_3, c_5, c_7, w_1, w_2),$$

some some arbitrary function φ, provided that $P_1 = A\varphi$ is a polynomial in its eight arguments. Here we use w_1 and w_2 in preference to c_4 and c_6.

TABLE A1. *The first integrals of the homological equation.*

c_1	$A\bar{A}$
c_2	$\frac{iB}{A} + \log(A)$
c_3	$i(A\bar{B} - \bar{A}B)$
c_4	$\frac{C}{A} - i\frac{B}{A}\log(A) - \frac{1}{2}(\log(A))^2$
c_5	$A\bar{C} - B\bar{B} + \bar{A}C$
c_6	$-i\frac{D}{A} - \frac{C}{A}\log(A) + i\frac{B}{2A}(\log(A))^2 + \frac{1}{6}(\log(A))^3$
c_7	$i(A\bar{D} - B\bar{C} + \bar{B}C - \bar{A}D)$
w_1	$-\frac{1}{A^2}\left(B^2 - 2AC\right)$
w_2	$-\frac{i}{A^2}\left((3AD - BC) + \frac{B}{A}\left(B^2 - 2AC\right)\right)$

In the derivation of the normal form for the Hamiltonian–Hopf bifurcation, the equivalent equation at this stage is $P_1(A, B, \bar{A}, \bar{B}) = A\varphi(c_1, c_2, c_3)$. The argument is then that φ is a polynomial in c_1 and c_3, and independent of c_2. This is because of the log dependence of c_2: as $A \to 0$, the logarithmic behaviour of c_2 does not match the polynomial behaviour of P_1, and thus φ must be independent of c_2. This argument follows through to our case as far as c_2 is concerned, but there are additional considerations regarding w_1 and w_2, which have A^2 in their denominators. This dependence in $A\varphi$ is eliminated by taking certain combinations of w_1 and w_2: for example, $Ac_1w_1 = -\bar{A}(B^2 - 2AC)$, which is fine, as is $A(c_1w_2 + w_1c_3) = \bar{A}(3AD - BC) + \bar{B}(B^2 - 2AC)$, while Ac_1w_2 has an A in the denominator and so is not a polynomial. In fact, only the two combinations c_1w_1 and $c_1w_2 + c_3w_1$ are needed for P_1 for $\frac{dA}{dx}$, but additional combinations appear in the other three equations.

After computing these and (re)labelling the arbitrary functions as P, Q, R and S, to be consistent with the notation of the normal form of the Hamiltonian–Hopf bifurcation (Burke & Knobloch, 2007a; Iooss & Adelmeyer, 1998), we have the eight-dimensional normal form

$$A_x = iA + B + iAP(c_1, c_3, c_5, c_7, w_1, w_2), \tag{A.10a}$$

$$B_x = iB + C + iBP(c_1, c_3, c_5, c_7, w_1, w_2) + AQ(c_1, c_3, c_5, c_7, w_1, w_2), \tag{A.10b}$$

$$\begin{aligned} C_x = {} & iC + D + iCP(c_1, c_3, c_5, c_7, w_1, w_2) + BQ(c_1, c_3, c_5, c_7, w_1, w_2) \\ & + iAR(c_1, c_3, c_5, c_7, w_1, w_2), \end{aligned} \tag{A.10c}$$

$$\begin{aligned} D_x = {} & iD + iDP(c_1, c_3, c_5, c_7, w_1, w_2) + CQ(c_1, c_3, c_5, c_7, w_1, w_2) \\ & + iBR(c_1, c_3, c_5, c_7, w_1, w_2) + AS(c_1, c_3, c_5, c_7, w_1, w_2). \end{aligned} \tag{A.10d}$$

The functions P, Q, R and S are understood to include only those combinations of w_1 and w_2 that result in polynomial contributions to the normal form. The nonlinear terms up to cubic order are:

$$P(c_1, c_3, c_5, c_7, w_1, w_2) = P_1c_1 + P_2c_3 + P_3c_5 + P_4c_7 + 3T_1(c_1w_2 + c_3w_1) - iT_2c_1w_1,$$

TABLE A2. *Relation between the normal coefficients in (A.9) and the normal form coefficients in (A.10).*

$\gamma_1 = iP_1$	$\gamma_2 = -P_2$	$\gamma_3 = iP_3$	$\gamma_4 = -P_4$	$\gamma_5 = -T_2$	$\gamma_6 = T_1$
$\gamma_7 = Q_1$	$\gamma_8 = iQ_2$	$\gamma_9 = Q_3$	$\gamma_{10} = iQ_4$	$\gamma_{11} = T_3$	$\gamma_{12} = -T_4$
$\gamma_{13} = iR_1$	$\gamma_{14} = -R_2$	$\gamma_{15} = iR_3$	$\gamma_{16} = -R_4$	$\gamma_{17} = T_5$	$\gamma_{18} = 2T_6$
$\gamma_{19} = -T_7/2$	$\gamma_{20} = S_1$	$\gamma_{22} = iS_2$	$\gamma_{22} = S_3$	$\gamma_{23} = iS_4$	$\gamma_{24} = T_8$
$\gamma_{25} = T_9$	$\gamma_{26} = T_{10}$				

$$\begin{aligned} Q(c_1, c_3, c_5, c_7, w_1, w_2) = {} & Q_1 c_1 + Q_2 c_3 + Q_3 c_5 + Q_4 c_7 + T_1(c_3 w_2 - 4c_5 w_1 + c_1 w_1^2) \\ & - iT_2 c_3 w_1 - T_3 c_1 w_1 - iT_4(c_3 w_1 + c_1 w_2), \end{aligned}$$

$$\begin{aligned} R(c_1, c_3, c_5, c_7, w_1, w_2) = {} & R_1 c_1 + R_2 c_3 + R_3 c_5 + R_4 c_7 \\ & + T_1(3c_7 w_1 - c_5 w_2 - 2c_1 w_1 w_2 - 2c_3 w_1^2) - iT_2(c_5 w_1 - c_1 w_1^2) \\ & - \tfrac{1}{2} T_3(c_1 w_2 - c_3 w_1) + iT_4(2c_3 w_2 - 3c_5 w_1 + 2c_1 w_1^2) \\ & + iT_5 c_1 w_1 + iT_6(c_3 w_2 - c_5 w_1 + c_1 w_1^2) - \tfrac{1}{2} T_7(c_1 w_2 + c_3 w_1), \end{aligned}$$

$$\begin{aligned} S(c_1, c_3, c_5, c_7, w_1, w_2) = {} & S_1 c_1 + S_2 c_3 + S_3 c_5 + S_4 c_7 \\ & + T_1(2c_1 w_2^2 - 3c_7 w_2 + 2c_3 w_1 w_2 + c_5 w_1^2) - iT_2(c_7 w_1 - c_3 w_1^2) \\ & - \tfrac{1}{2} T_3(c_3 w_2 - c_1 w_1^2) + iT_4(4c_1 w_1 w_2 + 4c_3 w_1^2 - 3c_5 w_2 - 6c_7 w_1) \\ & - iT_5 c_1 w_2 + iT_6(2c_1 w_1 w_2 + c_3 w_1^2 - 2c_5 w_2 + 3c_7 w_1) \\ & + \tfrac{1}{2} T_7(c_3 w_2 + c_1 w_1^2) - T_8 c_1 w_1 + T_9(c_3 w_2 - c_5 w_1 + c_1 w_1^2) \\ & + iT_{10}(c_3 w_1 + c_1 w_2), \end{aligned}$$

where the P_i, Q_i, R_i, S_i and T_j, $i = 1, \ldots, 4$, $j = 1, \ldots, 10$ are real coefficients (with the prefactor i included in the cases of T_2, T_4, T_5, T_6 and T_{10}). These terms may seem somewhat arbitrary, but are in fact very specific combinations to match the terms found by solving the homological equation (compare with (A.9)). The relation between the normal form coefficients here and the normal form coefficients in (A.9) is given in Table A.2.

Having found the terms present in the normal form, we now wish to find the coefficients of these terms. In the following sections, we will describe two methods to do this: by solving a linear system of equations derived from the system of ODEs (A.5), following Iooss & Adelmeyer (1998), and an asymptotic scaling method, following Burke & Knobloch (2007a).

A.3 *Determining the normal form coefficients I: Nonlinear coordinate transform*

We have so far described the linear transformation (A.7). Following Iooss & Adelmeyer (1998), we now add nonlinear terms to the transformation, in particular a polynomial $\boldsymbol{\Phi}(\tilde{\mathbf{z}})$, such that we have

$$\mathbf{z} = \zeta_0 A + \zeta_1 B + \zeta_2 C + \zeta_3 D + \bar{\zeta_0}\bar{A} + \bar{\zeta_1}\bar{B} + \bar{\zeta_2}\bar{C} + \bar{\zeta_3}\bar{D} + \boldsymbol{\Phi}(\tilde{\mathbf{z}}). \tag{A.11}$$

We fix $\boldsymbol{\Phi}$ such that it contains only quadratic and cubic terms. Substituting this into (A.5) and matching like powers of the variables results in a relationship between the parameters n_2 and n_3 in the model (A.4) and the normal form coefficients in (A.10):

$$\begin{aligned}
P_1 &= -\frac{1935}{5824}n_3 - \frac{6686165}{6368544}n_2^2, \qquad P_2 = -\frac{1418305}{1207224}n_2^2, \\
P_3 &= \frac{12194005}{6613488}n_2^2, \qquad P_4 = -\frac{6220189}{8424324}n_2^2, \\
Q_1 &= -\frac{75}{224}n_3 - \frac{61235}{81648}n_2^2, \qquad Q_2 = -\frac{645}{5824}n_3 - \frac{5539735}{6368544}n_2^2, \\
Q_3 &= \frac{2922859}{1810836}n_2^2, \qquad Q_4 = \frac{4594355}{6613488}n_2^2, \\
R_1 &= \frac{9}{32}n_3 + \frac{1483}{3888}n_2^2, \qquad R_2 = \frac{25}{224}n_3 + \frac{45649}{81648}n_2^2, \\
R_3 &= -\frac{135}{5824}n_3 - \frac{513995}{909792}n_2^2, \qquad R_4 = -\frac{923965}{1207224}n_2^2, \\
S_1 &= \frac{3}{16}n_3 + \frac{163}{648}n_2^2, \qquad S_2 = \frac{3}{32}n_3 + \frac{473}{3888}n_2^2, \\
S_3 &= -\frac{5}{224}n_3 - \frac{967}{3024}n_2^2, \qquad S_4 = -\frac{15}{5824}n_3 - \frac{918133}{6368544}n_2^2, \\
T_1 &= \frac{5400535}{2808108}n_2^2, \qquad T_2 = \frac{12625255}{4408992}in_2^2, \\
T_3 &= -\frac{2005877}{1810836}n_2^2, \qquad T_4 = -\frac{528565}{944784}in_2^2, \\
T_5 &= -\frac{225}{1456}in_3 - \frac{221885}{530712}in_2^2, \qquad T_6 = \frac{4026445}{6613488}in_2^2, \\
T_7 &= \frac{1142417}{1810836}n_2^2, \qquad T_8 = -\frac{5}{32}n_3 - \frac{815}{3888}n_2^2, \\
T_9 &= -\frac{1718057}{1810836}n_2^2, \qquad T_{10} = -\frac{135}{2912}in_3 - \frac{286375}{1061424}in_2^2.
\end{aligned} \tag{A.12}$$

All the normal form coefficients are either purely real or purely imaginary, which is a consequence of the reversibility symmetry.

A.4 *Determining the normal form coefficients II: Asymptotic scaling method*

This method involves expanding both the steady model equation (A.4) and the normal form equations (A.10) in powers of a small parameter ϵ, following Burke & Knobloch (2007a). The normal form coefficients can then be found by matching the equations at each order of ϵ.

A.4.1 *Model equation expansion.* We introduce a small parameter ϵ, and define a long length scale $X = \epsilon^{1/2}x$, as we did in the weakly nonlinear analysis in §3. We then expand $u(x)$ in terms of this small parameter, *i.e.*,

$$u(x) = \sum_{n=2}^{12} \epsilon^{n/2} u_n(x, X). \tag{A.13}$$

The summation index runs from $n = 2$ because the amplitude of u is $\mathcal{O}(\epsilon)$ (see §3). We need to go to $n = 12$ in order to determine all the coefficients in the normal form (A.10).

Substituting (A.13) into (A.4), we obtain equations to be solved at each order of $\epsilon^{1/2}$, *i.e.*,

$$\begin{aligned}
\mathcal{O}(\epsilon) : 0 &= -\left(1 + \partial_{xx}\right)^4 u_2 \equiv -\mathcal{L}u_2,\\
\mathcal{O}(\epsilon^{3/2}) : 0 &= -\mathcal{L}u_3 - 8\partial_{xX}\left(1 + \partial_x^2\right)^3 u_2,\\
\mathcal{O}(\epsilon^2) : 0 &= -\mathcal{L}u_4 - 8\partial_{xX}\left(1 + \partial_x^2\right)^3 u_3 - 4\partial_X^2\left(1 + 9\partial_x^2 + 15\partial_x^4 + 7\partial_x^6\right) u_2 + n_2 u_2^2,\\
\mathcal{O}(\epsilon^{5/2}) : 0 &= -\mathcal{L}u_5 - 8\partial_{xX}\left(1 + \partial_x^2\right)^3 u_4 - 4\partial_X^2\left(1 + 9\partial_x^2 + 15\partial_x^4 + 7\partial_x^6\right) u_3\\
&\quad - 8\partial_X^3\partial_X\left(3 + 10\partial_x^2 + 7\partial_x^4\right) u_2 + 2n_2 u_2 u_3,\\
\mathcal{O}(\epsilon^3) : 0 &= -\mathcal{L}u_6 - 8\partial_{xX}\left(1 + \partial_x^2\right)^3 u_5 - 4\partial_X^2\left(1 + 9\partial_x^2 + 15\partial_x^4 + 7\partial_x^6\right) u_4\\
&\quad - 8\partial_X^3\partial_X\left(3 + 10\partial_x^2 + 7\partial_x^4\right) u_3 - 2\partial_X^4\left(3 + 30\partial_x^2 + 35\partial_x^4\right) u_2\\
&\quad + n_2\left(u_3^2 + 2u_2 u_4\right) + n_3 u_2^3,
\end{aligned}$$

and similarly for higher orders, up to $\mathcal{O}(\epsilon^6)$. This analysis is equivalent to the one performed in §3, though there is a factor of two difference in the subscript of u between the two calculations.

The leading order solution is given by

$$u_2(x, X) = A_2(X)e^{ix} + c.c.,$$

and similarly from $\mathcal{O}(\epsilon^{3/2})$ we have

$$u_3(x, X) = A_3(X)e^{ix} + c.c..$$

In the weakly nonlinear analysis in §3, we set $u_{3/2} = 0$ (equivalently $u_3 = 0$ here); in this analysis we keep u_3 non-zero. The difference is of no consequence, however.

Proceeding to $\mathcal{O}(\epsilon^2)$, the ansatz $u_4 = \lambda_4 + A_4(X)e^{ix} + B_4(X)e^{2ix} + c.c.$, where λ_4 is real, leads to the solution

$$\lambda_4 = 2n_2|A_2|^2, \qquad B_4 = \frac{n_2}{81}A_2^2, \qquad \bar{B}_4 = \frac{n_2}{81}\bar{A}_2^2,$$

and $A_4, \bar{A}_4$ are as yet unknown. We have dropped the explicit X dependence for convenience. Again, this is exactly the solution found in §3; similarly the solution at $\mathcal{O}(\epsilon^{5/2})$ is as described in §3.

At $\mathcal{O}(\epsilon^3)$, this analysis begins to differ from the one in §3. In particular, whereas in §3 the time derivatives first appeared at $\mathcal{O}(\epsilon^3)$, here we have no time derivatives. Instead we obtain a fourth-order ODE for A_2, namely

$$16A_2'''' = \left(3n_3 + \tfrac{326}{81}n_2^2\right)|A_2|^2A_2,$$

where the prime denotes differentiation with respect to X. We note that the coefficient of the nonlinear term is n_A from (2.3). We obtain similar equations for the A_j, $j = 3, \ldots, 8$ at $\mathcal{O}(\epsilon^{2+j/2})$. For example, we find

$$16A_3'''' = \left(3n_3 + \tfrac{326}{81}n_2^2\right)\left(2|A_2|^2A_3 + A_2^2\bar{A}_3\right) + \frac{64}{243}in_2^2|A_2|^2A_2' + 32iA_2''''$$

at $\mathcal{O}(\epsilon^{7/2})$. Continuing this process up to $\mathcal{O}(\epsilon^6)$, we obtain all the required equations. We may then reconstitute these into one equation by defining

$$Z(X) = \sum_{n=2}^{8} \epsilon^{(n-2)/2}A_n(X).$$

The resulting equation has derivatives up to eighth order. However, derivatives higher than fourth order appear at higher order than the A'''' term, and these can be eliminated by repeatedly differentiating the resulting equation and substituting back in to the equation. The resulting equation is then

$$\begin{aligned} 16Z'''' = {} & \theta_1|Z|^2Z + \epsilon^{1/2}\left(\left(\theta_2 + 4i\theta_1\right)|Z|^2Z' + 2i\theta_1Z^2\bar{Z}'\right) + \epsilon\Big(-\frac{5}{2}\theta_1Z^2\bar{Z}'' \\ & + \left(2i\theta_3 - 5\theta_1 + \theta_3\right)\left(\bar{Z}(Z')^2 + |Z|^2Z''\right) + 2\left(i\theta_2 - 5\theta_1\right)ZZ'\bar{Z}'\Big) + \mathcal{O}(\epsilon^{3/2}), \end{aligned} \tag{A.14}$$

where the θ_i, $i = 1, \ldots, 3$ coefficients are

$$\theta_1 = 3n_3 + \frac{326}{81}n_2^2, \qquad \theta_2 = \frac{64}{243}in_2^2, \qquad \theta_3 = -\frac{592}{729}n_2^2.$$

To match to the scaled normal form equation (derived in the next section), we require one more transformation. This is

$$\begin{aligned} Z = {} & A + \epsilon^2\rho_1|A|^2A + \epsilon^{5/2}\left(\rho_2|A|^2A' + \rho_3A^2\bar{A}'\right) \\ & + \epsilon^3\left(\rho_4|A|^2A'' + \rho_5A^2\bar{A}'' + \rho_6\bar{A}(A')^2 + \rho_7AA'\bar{A}'\right), \end{aligned} \tag{A.15}$$

where the ρ_i, $i = 1, \ldots, 6$ coefficients are to be determined through the matching procedure. Under this transformation, (A.14) becomes

$$16A'''' = \theta_1|A|^2A + \epsilon^{1/2}\left(\left(\theta_2 + 4i\theta_1\right)|A|^2A' + 2i\theta_1A^2\bar{A}'\right) + \epsilon\Big(-\frac{5}{2}\theta_1A^2\bar{A}'' \\ + \left(2i\theta_3 - 5\theta_1 + \theta_3\right)\left(\bar{A}(A')^2 + |A|^2A''\right) + 2\left(i\theta_2 - 5\theta_1\right)AA'\bar{A}'\Big) + \mathcal{O}(\epsilon^{3/2}). \tag{A.16}$$

We have continued up to $\mathcal{O}(\epsilon^3)$, but the number of terms in (A.16) quickly escalates to such an extent that it is not instructive to include them all here; the truncated form of (A.16) is sufficient for the argument presented below.

A.4.2 *Normal form scaling.* To match the scaling in §A.4.1, we write

$$(A(X), B(X), C(X), D(X)) = (\epsilon\tilde{A}(X), \epsilon^{3/2}\tilde{B}(X), \epsilon^2\tilde{C}(X), \epsilon^{5/2}\tilde{D}(X))e^{ix},$$

where, as before, $X = \sqrt{\epsilon}x$, and we have factored out an e^{ix} dependence. With this, the normal form for A_x, (A.10a), becomes

$$A_x = \epsilon(i\tilde{A} + \sqrt{\epsilon}\tilde{A}_X)e^{ix} = \left(i\epsilon\tilde{A} + \epsilon^{3/2}\tilde{B} + i\epsilon\tilde{A}\epsilon P(\epsilon^2\tilde{c_1}, \epsilon^{5/2}\tilde{c_3}, \epsilon^3\tilde{c_5}, \epsilon^{7/2}\tilde{c_7}, \epsilon\tilde{w_1}, \epsilon^{3/2}\tilde{w_2})\right)e^{ix}.$$

Cancelling the common factor e^{ix}, subtracting $i\epsilon\tilde{A}$ from both sides and dropping the tildes, we have

$$\epsilon^{3/2}A_X = \epsilon^{3/2}B + i\epsilon^3P_1|A|^2A - \epsilon^{7/2}P_2A\left(A\bar{B} - \bar{A}B\right) + i\epsilon^4A\left(A\bar{C} - B\bar{B} + \bar{A}C\right) \\ - \epsilon^{9/2}P_4A\left(A\bar{D} - B\bar{C} + \bar{B}C - \bar{A}D\right) - \epsilon^4T_2\bar{A}\left(B^2 - 2AC\right) \\ + 3\epsilon^{9/2}T_1\left(\bar{A}\left(3AD - BC\right) + \bar{B}\left(B^2 - 2AC\right)\right). \tag{A.17}$$

We may cast this in appropriate form for the analysis by dividing through by a factor of $\epsilon^{3/2}$ and rearranging, such that we have

$$B = A_X + \mathcal{O}(\epsilon^{3/2}). \tag{A.18}$$

We do not explicitly write out all the terms for the sake of clarity in explaining the procedure.

Similarly, from (A.10) we have

$$C = B_X - \epsilon Q_1|A|^2A + \mathcal{O}(\epsilon^{3/2}) \tag{A.19}$$

and

$$D = C_X - i\epsilon^{1/2}R_1|A|^2A + \epsilon\left(R_2A^2\bar{B} - \left(Q_1 + R_2\right)|A|^2B\right) + \mathcal{O}(\epsilon^{3/2}). \tag{A.20}$$

We also obtain an equation for D_X, which we leave in the form

$$D_X = S_1|A|^2A + i\epsilon^{1/2}\left(S_2A^2\bar{B} + \left(R_1 - S_2\right)|A|^2B\right) \\ + \epsilon\Big(S_3A^2\bar{C} - \left(R_2 + S_3\right)AB\bar{B} + \left(R_2 + T_8\right)\bar{A}B^2 \\ + \left(S_3 + Q_1 - 2T_8\right)|A|^2C\Big) + \mathcal{O}(\epsilon^{3/2}). \tag{A.21}$$

The next step is to differentiate (A.18) with respect to X, giving

$$B_X = A_{XX} + \mathcal{O}(\epsilon^{3/2}). \tag{A.22}$$

Substituting (A.22) into (A.19), we have

$$C = A_{XX} - \epsilon Q_1 |A|^2 A + \mathcal{O}(\epsilon^{3/2}). \tag{A.23}$$

This procedure of differentiation and substitution is repeated twice more. Differentiating (A.23) with respect to X we have

$$C_X = A_{XXX} - \epsilon Q_1 \left(2|A|^2 A_X + A^2 \bar{A}_X\right) + \mathcal{O}(\epsilon^{3/2}). \tag{A.24}$$

Before substituting (A.24) into (A.20), we first replace the B and $\bar{B}$ terms using (A.18). This yields

$$D = C_X - i\epsilon^{1/2} R_1 |A|^2 A + \epsilon \left(R_2 A^2 \bar{A}_X - \left(Q_1 + R_2\right) |A|^2 A_X\right) + \mathcal{O}(\epsilon^{3/2}). \tag{A.25}$$

Now substituting (A.24) into (A.25) we have

$$\begin{aligned} D &= A_{XXX} - \epsilon Q_1 \left(2|A|^2 A_X + A^2 \bar{A}_X\right) - i\epsilon^{1/2} R_1 |A|^2 A \\ &\quad + \epsilon \left(R_2 A^2 \bar{A}_X - \left(Q_1 + R_2\right) |A|^2 A_X\right) + \mathcal{O}(\epsilon^{3/2}) \\ &= A_{XXX} - i\epsilon^{1/2} R_1 |A|^2 A + \epsilon \left(\left(R_2 - Q_1\right) |A|^2 A_X - \left(R_2 + 3Q_1\right) A^2 \bar{A}_X\right) + \mathcal{O}(\epsilon^{3/2}). \end{aligned} \tag{A.26}$$

Differentiating one final time, we have

$$\begin{aligned} D_X = A_{XXXX} &- i\epsilon^{1/2} R_1 \left(2|A|^2 A_X + A^2 \bar{A}_X\right) + \epsilon \left(\left(R_2 - 5Q_1\right) A A_X \bar{A}_X \right. \\ &\left. + \left(R_2 - Q_1\right) A^2 \bar{A}_{XX} - \left(R_1 + 3Q_1\right) \left(\bar{A} A_X^2 + |A|^2 A_{XX}\right)\right) + \mathcal{O}(\epsilon^{3/2}). \end{aligned} \tag{A.27}$$

We now notice that we have two equations for D_X, (A.21) and (A.27), and thus equating the two will yield an equation for A_{XXXX}. Before we do this, we first should use (A.22) and (A.23) to replace the B, $\bar{B}$, C and $\bar{C}$ terms in (A.21). This gives

$$\begin{aligned} D_X = S_1 |A|^2 A &+ i\epsilon^{1/2} \left(S_2 A^2 \bar{A}_X + \left(R_1 - S_2\right) |A|^2 A_X\right) \\ &+ \epsilon \left(S_3 A^2 \bar{A}_{XX} - \left(R_2 + S_3\right) A A_X \bar{A}_X + \left(R_2 + T_8\right) \bar{A} A_X^2 \right. \\ &\left. + \left(S_3 + Q_1 - 2T_8\right) |A|^2 A_{XX}\right) + \mathcal{O}(\epsilon^{3/2}). \end{aligned} \tag{A.28}$$

Equating (A.27) and (A.28), we find

$$\begin{aligned} A_{XXXX} = S_1 |A|^2 A &+ \epsilon^{1/2} i((3R_1 - S_2)|A|^2 A_X + (S_2 + R_1) A^2 \bar{A}_X) \\ &+ \epsilon((2R_2 + T_8 + 3Q_1)\bar{A} A_X^2 + (5Q_1 - 2R_2 - S_3) A A_X \bar{A}_X \\ &+ (4Q_1 + S_3 + R_2 - 2T_8)|A|^2 A_{XX} + (S_3 + Q_1 - R_2) A^2 \bar{A}_{XX}) + \mathcal{O}(\epsilon^{3/2}). \end{aligned} \tag{A.29}$$

As in §A.4.1, continuing up to $\mathcal{O}(\epsilon^3)$ yields a very large number of terms, so we truncate at the same order as (A.16). This is sufficient for the coefficient matching in the next section.

A.4.3 *Order-by-order matching.* We now match the two equations (A.16) and (A.29) at each power of $\epsilon^{1/2}$ to recover the normal form coefficients. The subscript X in (A.29) and superscript prime in (A.16) are now equivalent. At leading order the solution is immediately recovered, and we have

$$S_1 = \frac{3}{16}n_3 + \frac{163}{648}n_2^2.$$

This is the same as calculated via the nonlinear coordinate transform method, as given in (A.12).

Proceeding to $\mathcal{O}(\epsilon^{1/2})$ we have to solve the equations

$$2i\theta_1 = i\left(R_1 + S_2\right), \qquad \theta_2 + 4i\theta_1 = i\left(3R_1 + S_2\right).$$

The solution to these two equations is

$$R_1 = \frac{9}{32}n_3 + \frac{1483}{3888}n_2^2, \qquad S_2 = \frac{3}{32}n_3 + \frac{473}{3888}n_2^2,$$

again, the same as (A.12).

At the next order, $\mathcal{O}(\epsilon)$, we have the four equations

$$\begin{aligned}
-\frac{5}{2}\theta_1 &= S_3 + Q_1 - R_2,\\
2i\theta_2 - 5\theta_1 + \theta_3 &= 4Q_1 + S_3 + R_2 - 2T_8,\\
2i\theta_2 - 5\theta_1 + \theta_3 &= 2R_2 + T_8 + 3Q_1,\\
2\left(i\theta_2 - 5\theta_1\right) &= 5Q_1 - 2R_2 - S_3.
\end{aligned}$$

Solving these four equations simultaneously, we find

$$\begin{aligned}
Q_1 &= -\frac{75}{224}n_3 - \frac{37907}{81648}n_2^2, \qquad R_2 = \frac{25}{224}n_3 + \frac{10657}{81648}n_2^2,\\
S_3 &= -\frac{5}{224}n_3 - \frac{103}{3024}n_2^2, \qquad T_8 = -\frac{5}{32}n_3 - \frac{815}{3888}n_2^2.
\end{aligned}$$

Comparing with (A.12), we see that there is a disagreement in three out of the four terms. T_8 agrees, whereas the other three agree only in the dependence on the cubic nonlinearity coefficient n_3.

The differences in Q_1, R_2 and S_3 are $2n_2^2/7$, $-3n_2^2/7$, $2n_2^2/7$ respectively. This trend continues at higher orders, *i.e.*, the normal form coefficients found by the asymptotic scaling method agree with those found by the nonlinear coordinate transform method only in the dependence on n_3. We note that any extra terms included in the transformation (A.15) to try and rectify this would depend on θ_1, and thus change the n_3-dependence of the normal form coefficients.

A possible explanation for this discrepancy is the non-uniqueness of the normal form. In the analysis of the Swift–Hohenberg equation, the equivalent linear transformation to (A.7) is more generally a two-parameter family of transformations (Burke & Knobloch, 2007a). Fixing the value of these parameters at linear order determines the values of the normal form coefficients at higher order. By extension, we similarly will have a four-parameter family of transformations. Whereas in the Hamiltonian–Hopf case setting these parameters to determine the linear coordinate transform automatically determines the normal form coefficients at higher order, that is not necessarily the case here. There may be extra parameters that have implicitly been set differently by the two different methods.

Similarly, it is possible the w_1 and w_2 terms could have introduced an extra hidden parameter into the system, and the value of this parameter chosen by the two methods is not consistent.

A.5 *First integrals of the normal form*

The normal form for the Hamiltonian–Hopf bifurcation has two integrals that allow one to determine geometrically the solutions of the Swift–Hohenberg equation (Iooss & Adelmeyer, 1998; Iooss & Pérouème, 1993; Woods & Champneys, 1999). So, for the normal form in our case to be of any use, we need to find integrals of the normal form (A.10).

One of the integrals of the normal form for the Hamiltonian–Hopf bifurcation is also an integral of the characteristic system used to derive the normal form. Why this should be the case is not obvious. Nonetheless, we might hope that one of the integrals (or some combination of the integrals) in Table A.1 is also be an integral for the normal form (A.10).

We first concentrate on the linear terms of the normal form (A.8), and consider the integral $c_7 = i\left(A\bar{D} - B\bar{C} + \bar{B}C - \bar{A}D\right)$. Differentiating c_7 with respect to x, we have

$$\begin{aligned}\frac{dc_7}{dx} &= \frac{d}{dx}\left(A\bar{D} - B\bar{C} + \bar{B}C - \bar{A}D\right)\\ &= A\frac{d\bar{D}}{dx} + \bar{D}\frac{dA}{dx} - B\frac{d\bar{C}}{dx} - \bar{C}\frac{dB}{dx} + C\frac{d\bar{B}}{dx} + \bar{B}\frac{dC}{dx} - \bar{A}\frac{dD}{dx} - D\frac{d\bar{A}}{dx}\\ &= A\left(-i\bar{D}\right) + \bar{D}\left(iA + B\right) - B\left(-i\bar{C} + \bar{D}\right) - \bar{C}\left(iB + C\right) + C\left(-i\bar{B} + \bar{C}\right)\\ &\quad + \bar{B}\left(iC + D\right) - \bar{A}\left(iD\right) - D\left(-i\bar{A} + \bar{B}\right)\\ &= 0,\end{aligned}$$

using (A.8). Thus c_7 is an integral of the linear normal form (A.8). There are three similar integrals of the linear normal form, to wit

$$\begin{aligned}\frac{d}{dx}\left(B\bar{D} - C\bar{C} + \bar{B}D\right) &= B\left(-i\bar{D}\right) + \bar{D}\left(iB + C\right) - C\left(-i\bar{C} + \bar{D}\right) - \bar{C}\left(iC + D\right)\\ &\quad + \bar{B}\left(iD\right) + D\left(-i\bar{B} + \bar{C}\right) = 0,\end{aligned}$$

$$\frac{d}{dx}\left(C\bar{D} - \bar{C}D\right) = C\left(-i\bar{D}\right) + \bar{D}\left(iC + D\right) - \bar{C}\left(iD\right) - D\left(-i\bar{C} + \bar{D}\right) = 0,$$

and

$$\frac{d}{dx}|D|^2 = D\left(-i\bar{D}\right) + \bar{D}\left(iD\right) = 0.$$

However, none of these four integrals of the linear normal form are integrals of the nonlinear normal form, nor is any combination of them. This failure to extend to the nonlinear normal form is entirely down to the presence of the w_1 and w_2 terms in the normal form. In particular, it is the fact that w_1 and w_2 are not real that the extension fails. A wider search for other possible forms for integrals did not uncover any.

The absence of integrals of the normal form prevents the extension of the geometric analysis of the Hamiltonian–Hopf bifurcation to our degenerate situation. A possible explanation for the lack of integrals of the normal form is the non-uniqueness of the normal form: other choices of which terms to keep in the polynomial $\mathbf{P}$ in (A.2) might lead to an integrable normal form. It would be interesting to pursue this further.